Geochemical Evolution within the Tonga–Kermadec–Lau Arc–Back-arc Systems: the Role of Varying Mantle Wedge Composition in Space and Time

A. EWART*, K. D. COLLERSON, M. REGELOUS, J. I. WENDT AND Y. NIU

DEPARTMENT OF EARTH SCIENCES, THE UNIVERSITY OF QUEENSLAND, BRISBANE, QLD. 4072, AUSTRALIA

New trace element and Sr, Nd, and Pb isotope data for lavas from the active Tonga–Kermadec arc in the southwest Pacific, the volcano of Niua fo'ou in the back-arc Lau Basin, and Pacific Ocean sediments from DSDP Sites 204 and 275, and ODP Site 596, are integrated with existing geochemical data for lavas from the Lau Basin, Samoa, the Louisville Ridge Seamount Chain (LR-SMC) and the extinct Lau Ridge arc, giving new insights into the petrogenesis of lavas in an active arc–back-arc system. Geochemical variations in Tonga–Kermadec arc lavas are the result of (1) differences in the amount and composition of the material being subducted along the arc, and (2) pre-existing heterogeneities in the upper mantle. Differences in the material being subducted beneath the arc have an important influence on the chemistry of the arc lavas. At the Kermadec Trench, ~1 km thick layer of sediment is being subducted beneath the arc, compared with ~200 m at the Tonga Trench. This results in the high Th/U and more radiogenic Pb isotope compositions of Kermadec lavas compared with Tonga lavas. The latter have Pb isotope compositions intermediate between those of Pacific sediments and Pacific mid-ocean ridge basalt (MORB), suggesting that much of the Pb in these lavas is derived from subducting Pacific Ocean crust. This is supported by the Pb isotope signatures of the subducting LR-SMC, which are also observed in lavas from the northern Tongan islands of Tafahi and Niuatoputapu. High field strength element (HFSE) and heavy rare earth element (HREE) concentrations are generally lower in Tongan lavas (particularly those from northern Tongan islands) than in Kermadec lavas. The Tonga Ridge basement, the proto-Tonga arc lavas (ODP Site 839) and the older Lau Ridge arc lavas are generally less depleted than the modern arc lavas. In the back-arc region, upper-mantle depletion as inferred from HFSE and HREE contents of the lavas broadly increases eastwards across the Lau Basin, whereas the subduction signature and volatile (CO$_2$ and F) contents increase eastwards towards the modern arc. These observations suggest that depletion is due to melt extraction during back-arc extension and volcanism, together with a long 'residence time' of mantle material within the mantle wedge. The upper mantle beneath the northernmost end of the Tonga arc and Lau Basin contains an ocean-island basalt (OIB) component derived from the Samoa plume to the north. This is reflected in high concentrations of Nb relative to other HFSE in lavas from Niua fo'ou, and Tafahi and Niuatoputapu islands at the northern end of the Tonga arc. Pb isotopes also suggest an LR-SMC contribution into Tafahi and Niuataputapu. Trace element and isotope modelling is used to investigate the combined effects of varying mantle source depletion and subduction on the geochemistry of the arc lavas. The results suggest that the arc lava geochemistry can be explained largely by the balance between a relatively constant subduction input of Pb, Th, U, Cs, Ba, Sr, Rb, K and Sc [corresponding to 0·001–0·005 weight fraction of the Stolper & Newman (1994, Earth and Planetary Science Letters, 121, 293–325] 'H$_2$O-rich component' composition), into the overlying, but variably depleted mantle wedge.

*Corresponding author.

INTRODUCTION

The Tonga–Kermadec island arc system extends for >3000 km NNE from New Zealand, located along part of the modern convergent margin created by the westward subduction of the Pacific Plate beneath the Australasian plate (Fig. 1). The arc is divided into northern (Tonga) and southern (Kermadec) segments by the intersection of the Louisville Ridge seamount chain (LR-SMC) with the trench. Subduction of this aseismic ridge has progressively moved southwards along the Tongan (Tofua) arc during the past ~5 my (Yan & Kroenke, 1993). The point of present impact is marked by the absence of both seismicity and volcanicity, and shallowing of the trench; the ages of the seamounts close to the modern trench are 66 Ma (Cheng et al., 1987). Convergence rates increase northwards from 5·1–5·3 (Kermadec) to 7·5 cm/yr (Tonga; Jarrard, 1986; DeMets et al., 1990). West of the Tonga–Kermadec arc lie the Lau Basin and the Havre Trough, both active back-arc basin systems. The Lau Basin has been the focus of recent intensive studies, notably the cruises of the R.V. *Sonne* (e.g. von Stackelberg & Shipboard Scientific Party, 1985; Boespflug et al., 1990; Sunkel, 1990) and Ocean Drilling Program Leg 135 (Hawkins et al., 1994). Gamble et al. (1993, 1995) and Gamble & Wright (1995) have reviewed the available data on the Havre Trough. The Lau–Tonga–Havre–Kermadec system represents the present configuration of the continuous migration of arc and back-arc volcanism and tectonism eastwards during the past 100 my, leading to fragmentation of eastern Australasia in the SW Pacific (Yan & Kroenke, 1993).

The Lau Basin, in common with other western Pacific back-arc basins, combines, within a relatively restricted zone, sea-floor spreading and adjacent convergent margin volcanism. This is reflected geochemically in the gradational characteristics from arc-like (Tonga–Kermadec lavas) to N-MORB-like (older, western Lau Basin lavas). There is also a tendency for the more arc-like lavas to be less magnesium rich, with the notable exception of the northern Tongan boninites (Falloon et al., 1987, 1989; Falloon & Crawford, 1991).

Lau Basin opening began before 6 Ma (Hawkins et al., 1994), and has occurred in two phases, an early 'basin and range' style rifting (referred to as 'older' Lau Basin in this paper), followed ~2 my ago by propagator-driven spreading ('new' Lau Basin). The southward migration of these propagators has produced the Central, Intermediate, and Eastern Lau spreading centres (CLSC, ILSC, and ELSC respectively), the southern tip of the latter forming the active Valu Fa Ridge (VF; Jenner et al., 1987; Vallier et al., 1991), which is converging on the southern end of the Tongan arc (Fig. 1). The opening of the Lau Basin has caused clockwise rotation of the Tongan ridge (Sager et al., 1994) and the splitting of the

formerly continuous Lau–Colville and Tonga–Kermadec ridges (Karig, 1970). The two-stage Lau Basin opening has special geochemical interest in that each stage is characterized by basaltic volcanism having different Pb isotopic compositions, lavas from the early phase having 'Pacific' MORB type Pb isotope compositions, and the later phase having an 'Indian' MORB signature (Hergt & Hawkesworth, 1994; Hickey-Vargas et al., 1995).

The Tonga–Kermadec arc lavas comprise a suite of low-K tholeiites, basaltic andesites, and less abundant andesites, dacites and rhyolites. Boninites occur on the northernmost termination of the Tongan ridge (Falloon et al., 1987, 1989; Falloon & Crawford, 1991; Danyushevsky et al., 1995). On the remnant Lau Ridge, three phases of volcanicity are recognized; the Lau Volcanic Group (LVG) from 14 to 5·4 Ma (overlapping early Lau Basin opening), the Korabasaga Volcanic Group (KVG) from 4·4 to 2·4 Ma, and the Mago Volcanic Group (MVG), <2·2 Ma (Cole et al., 1990). Lavas from the two earlier volcanic phases have arc-like geochemistry, whereas the youngest phase is alkalic and intraplate in geochemical affinities.

This paper considers the arc and back-arc as coupled systems, requiring convection and recycling of asthenosphere within the mantle wedge (Ewart & Hawkesworth, 1987; Ewart et al., 1994a). Magma generation is inferred to occur in the mantle wedge, presumably as a result of decompression melting, and facilitated by fluid movement from the subduction zone (Pearce & Parkinson, 1993; Pearce & Peate, 1995). As noted by these workers (following Tatsumi et al., 1986; Davies & Bickle, 1991; Davies & Stevenson, 1992), the extent of melting reflects the combination of depression of mantle solidus, extent of adiabatic upwelling above the solidus, and the composition of the mantle before melting. Fluid movement from the subduction zone is considered responsible for metasomatism within the mantle wedge, leading to the distinctive enrichment of large-ion lithophile elements (LILE) relative to high field strength elements (HFSE) and heavy rare earth elements (HREE) in arc and near-arc magmas. Ewart & Hawkesworth (1987) and Ewart et al. (1994a) explained the observed strong HFSE depletion within the arc lavas as due to melt extraction during back-arc extension.

AIMS AND SCOPE

This work presents new Sr, Nd and Pb isotope data, and trace element concentrations determined by inductively coupled plasma mass spectrometry (ICP-MS) for lavas from the Tonga and Kermadec island arcs. These data complement the extensive geochemical data available for Lau Basin lavas [Hawkins et al. (1994) and references therein]. Notwithstanding the intensive research carried

Fig. 1. Tonga–Kermadec Arc and Lau Basin–Havre Trough, showing locations and major tectonic features. The numbers 834–839 refer to ODP sites (Leg 135). Tonga and Kermadec islands are numbered: 1, Tafahi; 2, Niuatoputapu; 3, Fonualei; 4, Late; 5, Metis; 6, Kao; 7, Tofua; 8, Hunga Ha'apai and Hunga Tonga; 9, Eua; 10, Ata; 11, Raoul Group; 12, Macauley; 13, Curtis; 14, L'Esperance; 15, Niua fo'ou. Other abbreviations: PR, Peggy Ridge; KTJ, Kings Triple Junction; CLSC, ILSC and ELSC, Central, Intermediate and East Lau Spreading Centres; VF, Valu Fa Ridge. Inset shows DSDP Sites 204 and 275, and ODP Site 596. Bathymetry contours in metres.

out on western Pacific arc volcanism in recent years, numerous fundamental petrogenetic problems remain poorly understood. The aims of this study are:

(1) To integrate the new geochemical data for Tonga–Kermadec arc lavas with existing data for lavas from the Lau Basin, so as to examine variations of chemistry across the arc–back-arc transition. Geochemical gradients may provide insight into the mechanisms of fluid addition from the subducted slab to the mantle wedge, and the composition of the fluid component responsible for the distinctive geochemistry of arc lavas (Stolper & Newman, 1994; Pearce & Peate, 1995), which is still poorly constrained.

(2) To document along-arc variations of chemistry in the arc lavas. If back-arc magmatism is responsible for depletion within the mantle source of the arc lavas, then the extent of depletion of 'conservative' incompatible elements (Pearce & Parkinson, 1993) should increase northwards along the arc, reflecting the northward increase in the extent of back-arc spreading. In addition, along-arc geochemical variations in 'non-conservative' elements might be linked to differences in the material being subducted along the arc.

(3) To evaluate any temporal variation in arc lava geochemistry. The active Tonga–Kermadec arc represents the most recent phase of arc magmatism in this

region. Volcanism on the Lau–Colville–Three Kings arc systems dates back to ~25 Ma (Yan & Kroenke, 1993). The recent Tonga–Kermadec lavas, erupted since the onset of back-arc spreading, may therefore be more strongly depleted in highly incompatible elements, relative, for example, to the older Lau Ridge arc lavas, or the 'proto'-Tongan arc (ODP Site 839; Ewart et al., 1994b).

(4) To use new sediment analyses to determine the extent to which sediments and subducted altered oceanic crust contribute to the trace element budget of arc magmatism. The degree of sediment recycling at subduction zones and the proportion of 'new' crust that is formed from the mantle at convergent plate margins are important parameters in the Earth's continuing geochemical evolution. Variations in volatile (CO_2, F, H_2O) abundances and slab-derived elements such as Ba, Cs, U, Pb and Th, in conjunction with isotope data, can provide insights into the source(s) of the trace elements.

(5) To examine the extent to which OIB sources influence the chemistry of the arc lavas. The Samoan plume lies ~200 km from the northern end of the Tonga arc, and geophysical studies (Giardini & Woodhouse, 1986) suggest a southerly movement of upper-mantle material beneath the northern Lau Basin. The mantle plume responsible for magmatism on the subducting LR-SMC is at present located close to the Heezen Fracture Zone in the southern Pacific, but subduction of the 70–90-my-old Louisville seamounts beneath the northern Tonga arc also plausibly has an influence on the chemistry of arc magmatism.

(6) To re-evaluate the petrogenesis of the enigmatic active subaerial volcano of Niua fo'ou in the northern Lau Basin. Olivine tholeiites erupted on Niua fo'ou have MORB-like major element chemistry, but possess trace element and isotopic compositions distinct from other regional back-arc and arc lavas (Reay et al., 1974; Ewart & Hawkesworth, 1987; Ewart et al., 1994a).

SAMPLES AND PROCEDURES

Sixty-three lavas from the Tonga and Kermadec arcs have been analysed for Pb and Sr isotopes, 23 for Nd isotopes, and 58 for trace elements using ICP-MS. These data supplement and update earlier data for the arc lavas (Ewart et al., 1973, 1977, 1994a, 1994b; Ewart & Hawkesworth, 1987), and complement the Lau Ridge and Basin data presented by Hawkins et al. (1994). The lavas analysed are from 15 islands along the length of the arc, and including the back-arc volcano of Niua fo'ou (Fig. 1). In addition, trace element and isotope data have been obtained for 15 samples of sediment from DSDP Sites 204 and 275 and ODP Site 596 (see Fig. 1), to constrain the effect of sediment subduction on the

chemistry of the arc magmatism. The sediment data in Table 3 (below) have been normalized on an anhydrous basis. Geochemical data for the LR-SMC and Samoan lavas are from Cheng et al. (1987) and Hawkins & Lonsdale (1987) (LR-SMC), and Newsom et al. (1986), Palacz & Saunders (1986), Wright & White (1987) and Farley et al. (1992) (Samoa).

In some of the diagrams in this paper, data from individual Tongan and Kermadec volcanoes, Lau Ridge volcanic phases, and certain subregions within the Lau Basin (e.g. VF, ELSC, CLSC, and individual ODP sites) are presented normalized to 6% MgO, to minimize the geochemical effects of low-pressure fractional crystallization, which has modified the compositions of most, if not all lavas (e.g. Ewart et al., 1973, 1994a, 1994b). This has been achieved by regressing the available data for each location to 6% MgO, except for lavas from Tofua and Ata islands where, because of insufficient data, a regression line calculated from the average of all the Tonga data is used.

Analytical techniques

Isotopic analyses

Sediment samples were rinsed several times in distilled water in an ultrasonic bath before digestion. Isotope analyses of lavas were carried out on crushed handpicked whole-rock chips. Samples were dissolved in HF–HNO_3 and brought into solution in HCl. Sr and the REE were separated on cation ion exchange resin, Nd was then separated from the other REE using a conventional bis-(2-ethylhexyl)hydrogen phosphate (HDEHP) method. All reagents used were quartz-distilled. Pb was separated from the rock matrix using a technique modified after Manhes et al. (1978); blanks for the entire procedure were <0·3 ng. All isotope analyses were carried out on a Fisons VG54-30 Sector thermal ionization mass spectrometer. Sr and Nd were analysed in multicollector dynamic mode, and corrected for fractionation using $^{86}Sr/^{88}Sr = 0·1194$ and $^{146}Nd/^{144}Nd = 0·7219$. Mean values for the NBS987 Sr and La Jolla Nd standards over the period of analysis were $0·710240 \pm 24$ and $0·511857 \pm 14$ (2σ), respectively. Table 1 presents the results for the Tonga–Kermadec lavas.

Major and trace elements

Major elements were analysed by X-ray fluorescence, following the methods described by Norrish & Hutton (1969). Trace element concentrations were determined by ICP-MS. Samples were crushed in agate into fine grains (500–1000 μm, depending on the grain size of the constituent minerals); where possible powders were avoided, to minimize contamination. Samples were leached in 10% H_2O_2–5% HCl for 10 min at room

Table 1: New isotopic determinations of lavas from the Tonga and Kermadec arc, and Niua fo'ou island, Lau Basin

Sample	$^{87}Sr/^{86}Sr$	$^{143}Nd/^{144}Nd$	$^{206}Pb/^{204}Pb$	$^{207}Pb/^{204}Pb$	$^{208}Pb/^{204}Pb$
1. Tonga					
Hunga Ha'apai and Hunga Tonga					
HHBF	0·703764	0·512958	18·651	15·574	38·293
HHMF	0·703694	—	18·648	15·565	38·268
HHUF	0·703527	0·513051	18·649	15·584	38·308
38983	0·703647	—	—	—	—
38984	0·703740	—	18·619	15·573	38·263
Tofua					
Tof32	0·703503	0·513022	18·640	15·582	38·291
Kao					
104C	0·703196	0·513036	18·602	15·572	38·224
64T4C	0·703263	—	18·622	15·570	38·236
64T6	0·703271	—	18·616	15·571	38·229
T101P	0·703344	—	18·602	15·560	38·196
T102	0·703289	—	18·518	15·571	38·164
T103C	0·703337	0·513035	18·651	15·574	38·293
Metis Shoal					
11108	0·703643	0·513032	18·562	15·567	38·214
Late					
L13	0·703644	—	18·579	15·573	38·225
L20	0·703547	—	18·603	15·583	38·279
L21	0·703822	0·512968	18·571	15·559	38·199
L3	0·703666	0·512981	18·590	15·548	38·129
L7	0·703612	—	18·570	15·566	38·194
Fonualei					
F20	0·703721	—	18·597	15·554	38·229
F30	0·703510	0·512966	18·589	15·578	38·271
F31	0·703919	0·512966	18·589	15·578	38·271
F39	0·703774	—	18·609	15·573	38·285
F41	0·703819	0·512966	18·573	15·548	38·200
F8	0·703833	0·512953	18·580	15·549	38·189
Niuatoputapu					
NT051	0·703978	—	19·250	15·623	38·956
NT052a	0·704040	—	19·209	15·621	38·934
NT053	0·704006	—	19·003	15·602	38·742
NT054	0·704035	—	19·258	15·621	38·965
NT64-T2	0·704094	—	19·005	15·618	38·780
NT64-T8	0·704073	—	18·925	15·605	38·672
Tafahi					
T068	0·703898	—	19·311	15·629	38·964
T069	0·703924	—	19·041	15·592	38·682
T072	0·703898	—	19·258	15·618	38·900
T073	0·703930	—	18·926	15·593	38·608
T113	0·704300	0·512896	19·306	15·619	38·934
T114	0·703992	0·512956	19·103	15·612	38·782
T116	0·703992	0·512940	18·970	15·600	38·632

Table 1: continued

Sample	^{87}Sr/^{86}Sr	^{143}Nd/^{144}Nd	^{206}Pb/^{204}Pb	^{207}Pb/^{204}Pb	^{208}Pb/^{204}Pb
2. Lau Basin					
Niua fo'ou					
N107	0·704181	0·512809	18·413	15·602	38·493
N108	0·704233	—	18·460	15·613	38·543
N110	0·704366	0·512797	18·465	15·603	38·564
N111	0·704342	0·512822	18·410	15·585	38·459
N131	0·704365	—	18·369	15·580	38·394
3. Kermadecs					
L'Esperance					
14831	—	—	18·789	15·629	38·655
14835	0·704041	0·512988	18·696	15·587	38·493
14837	0·704019	0·512967	18·706	15·618	38·564
14840	0·704393	0·512987	18·716	16·616	38·575
Curtis					
14849	0·704097	0·513014	18·739	15·619	38·597
14864	0·704077	0·513011	18·724	15·620	38·615
14868	0·704444	—	18·651	15·595	38·496
Macauley					
10378	0·703360	—	18·657	15·588	38·362
10379	0·703469	0·513007	18·528	15·564	38·232
10380	0·703499	—	18·635	15·589	38·389
10384	0·703705	0·513031	18·699	15·589	38·452
10415	0·703504	0·513053	18·671	15·587	38·406
Raoul Group					
14775	0·704122	0·513066	18·709	15·586	38·479
14782	0·703604	0·513004	18·629	15·579	38·368
14790	0·703605	0·513046	18·590	15·594	38·380
14796	0·703612	0·513068	18·633	15·578	38·373
23374	0·703466	—	18·680	15·592	38·432
23376	0·703384	0·513053	18·719	15·586	38·428
23383	0·703755	—	18·686	15·586	38·437
23386	0·703552	—	18·700	15·599	38·403
7101	0·703528	0·513035	18·538	15·583	38·266

Average within-run 2σ errors for ^{87}Sr/^{86}Sr are 0·000010. For ^{143}Nd/^{144}Nd, 2σ errors are 0·000009. For Pb isotopic measurements, the fractionation correction factor is 1·4‰ per mass unit.

temperature to remove labile material on grain surfaces, and then rinsed several times with distilled water. ICP-MS analyses were carried out on a Fisons Plasma Quad 2 instrument; Niu & Hékinian (1997) have given full details of the analytical procedures. The new trace element data for Tonga–Kermadec lavas are given in the Appendix (Table A1).

Volatile analyses

H_2O determination used Karl Fischer titration (Turek *et al.*, 1976), with CO_2 analyses performed by non-aqueous titration against sodium methoxide, using thymol phthalein indicator (Turek *et al.*, 1978). Approximately 2·5 g of sample was used. Replicate analyses indicate reproducibility within $\pm$10%. Precision for H_2O was checked using the international standards JG1a (average value obtained 0·73%), JGb1 (average 1·47%), and copper sulphate pentahydrate (average 36·63%). CO_2 analyses were checked against the standard MA-N, which gave an average value of 1475 ppm.

F determinations were made with a fluoride ion-selective electrode after fusion with lithium metaborate (Bodkin, 1977), and concentrations were obtained by the

method of standard fluoride addition. Replicate analyses indicate reproducibility of within $\pm 10\%$ relative, at the abundance levels observed in the present sample set (see Appendix, Table A1).

SEDIMENTS

The sediments analysed (Table 2) are from two sites on Pacific oceanic crust to the east of the Tonga Trench (DSDP Site 204 and ODP Site 596), and from DSDP Site 275, close to the edge of the Campbell Plateau. Sediments from the latter site may thus be representative of continent-derived material, whereas the other two sites sample abyssal sediments with variable volcanogenic contributions. These data supplement those of Gamble *et al.* (1996) for sediments dredged from the Kermadec Trench and its hanging wall, the Hikurangi Trough (east of New Zealand), and the adjacent Pacific Plate.

(1) *Site 204 (Burns* et al., *1973)*. Unit 1 consists of 103 m of Early Miocene to Oligocene abyssal clays and ash, dominated by montmorillonite, feldspars, quartz, glass shards, iron oxides, augite, and zeolites. These are interpreted as deep water abyssal sediments containing a contemporaneous volcanic component, believed to be wind-transported from the developing precursor to the Tongan arc. Unit 2 is 23·5 m of ?Early Cretaceous, tuﬀaceous sandstones and conglomerates, containing clasts of calcite, plagioclase, volcanic glass, and basalt. Unit 3 (age uncertain) comprises 20·5 m of dark vitric tuﬀ consisting of devitrified basaltic glass, altered feldspar, and augite. Units 2 and 3 have been interpreted as accumulating on a topographic high near a basaltic source, probably the LR-SMC, a conclusion supported by the Pb isotopic data presented in this paper.

(2) *Site 596 (Menard* et al., *1987)*. Unit 1 consists of 11 m of Early Miocene and younger, zeolitic pelagic clays, containing clays, $\pm$feldspar, opaque micronodules, zeolites, biogenic traces, and semi-opaque oxides. Unit 2 comprises 16 m of Oligocene–Eocene to Cretaceous zeolitic metalliferous pelagic clays, containing a higher proportion of the semi-opaque oxides (the result of a very slow accumulation rate). Unit 3 comprises 41 m of Cretaceous sediments similar to Unit 2 with thin interbeds of pelagic clays, cherts and porcellanite.

(3) *Site 275 (Kennett* et al., *1974)*. Unit 1 comprises 13 m of sandy-silt radiolarian and diatom-bearing ooze, with the detrital component consisting of quartz, schistose and sedimentary fragments, glauconite, micas, chlorite, and feldspars. Unit 2 is represented by 39 m of a glauconite and micronodule-bearing clayey-silt, with a similar detrital component to Unit 1. Both units are Late Cretaceous in age, based on microfossil assemblages.

The sediments from the three sites are not strongly calcareous, and therefore less biogenic than those reported by Gamble *et al.* (1996), whereas the continental provenance of the Site 275 samples is clearly reflected in their detrital nature and chemical composition, compared with the more pelagic and volcanogenic sediments of Sites 204 and 596 (e.g. Fig. 2a and b). A significant aspect of the sediment chemistry is the variation with depth at each site (Fig. 2), with compositions being relatively similar at the surface (noting some provenance eﬀects at Site 275), but diverging markedly at each site with increasing depth. These trends are best illustrated by the ratios Al_2O_3/TiO_2, Nb/Yb, Ti/Y (Fig. 2b–d), Sc/Yb, Th/Yb and K/Cs. We interpret the relative similarities of the surface sediments to reflect the young volcanic ash components derived from the arc and its volcanically active extension in northern New Zealand. This implies that surface-dredged sediments may not reflect the compositions of the main subducted sediment column. For example, Gamble *et al.* (1996) have found systematically changing Pb, Sr and Nd isotopic compositions of sediments along the Kermadec arc and have shown these latitudinal variations to be mirrored in the chemistry of lavas from the volcanic islands along the arc. However, as these sediments were dredged, it is possible that variations in sediment composition reflect variations in volcanic detritus in the surface sediments close to the trench.

A second significant variation is the distinctive compositions (Fig. 2b–e) of the two deepest samples from Site 204 (Units 2 and 3). These were previously interpreted to consist of detrital volcanic material from the LR-SMC (Burns *et al.*, 1973), and this is confirmed by new Pb isotopic data (see also Fig. 6c and d, below). Other significant aspects of the sediment geochemistry include the following:

(1) The Site 275 sediments show closer aﬃnities to the Kermadec–Hikurangi sediment data (e.g. Sr and Pb isotopes, Al/Zr, Ba/Yb, Ce/Yb, Th/Y and Nb/Yb relations; see Gamble *et al.*, 1996) reflecting the continental detrital input.

(2) Sediment Th/U ratios of all three Sites are >2, up to 5, and thus closer to the Kermadec lavas than Tonga (mostly <2).

(3) REE are characterized by LREE enrichment (80–800 times chondritic for Site 596, 30–400 times for Site 204, and 70–80 times for Site 275), and exhibit negative Eu/Eu* anomalies (Fig. 2e), which vary systematically between sites; only the two lowest samples from Site 204 do not exhibit Eu anomalies. Three samples from Site 596 have negative Ce anomalies.

(4) Measured $^{87}Sr/^{86}Sr$ ratios are higher than for present-day seawater at Site 275 (continental detritus), but apart from the near-surface samples (which are close to

Table 2: Major element (wt %), trace element (ppm; ICP-MS), and isotopic compositions of selected sediments from DSDP Sites 204 and 275, and ODP Site 596

Site:	204	204	204	204	204	204	204	275	275	275	596	596	596	596	596
Core:	1	1	1	3	5	6	9	1	2	4	1	2	2	3	6
Section:	1	3	4	2	5	2	3	1	3	2	1	3	6	6	6
Interval (cm):	30–33	52–55	103–106	103–106	60–63	66–69	67–70	113–116	55–60	10–15	115–118	85–88	77–80	84–87	124–127
Depth (m):	0·3	3·52	5·53	50·53	100·60	105·16	144·67	1·13	8·57	35·10	1·15	9·35	13·77	23·44	48·54
Unit:	1	1	1	1	1	2	3	1	1	2	1	1	2	2	3B
SiO_2	56·3	55·5	57·1	59·9	49·6	46·9	48·1	78·2	79·5	78·1	54·7	52·5	44·5	54·0	87·5
TiO_2	0·93	0·90	0·86	0·93	1·05	2·22	2·29	0·38	0·43	0·55	0·93	1·10	0·67	0·66	0·12
Al_2O_3	16·19	17·52	15·86	14·52	16·06	12·31	11·91	6·71	7·34	10·37	17·06	17·77	12·95	15·22	3·34
$Fe_2O_3{}^*$	9·67	9·73	10·36	10·44	11·47	12·99	12·14	4·39	4·81	3·32	9·99	12·46	16·16	9·12	3·07
MnO	0·654	0·671	0·442	0·131	0·131	0·183	0·162	0·022	0·018	0·018	1·06	1·11	4·47	3·52	0·755
MgO	4·51	3·76	3·67	4·90	3·35	4·56	16·56	1·67	1·77	1·78	4·13	3·23	3·57	3·39	1·35
CaO	2·93	3·20	4·26	2·33	4·34	12·92	1·56	2·57	0·49	0·36	1·99	1·84	4·56	2·27	0·74
Na_2O	4·60	4·61	4·37	4·30	3·62	2·47	3·95	2·80	2·57	1·80	4·41	5·89	5·02	4·24	1·71
K_2O	2·56	2·50	1·60	1·49	3·33	3·20	1·29	2·19	2·58	2·52	3·16	2·88	2·34	2·27	0·82
P_2O_5	0·229	0·179	0·127	0·102	1·72	0·181	0·253	0·083	0·065	0·041	0·223	0·333	2·92	1·27	0·386
Total	98·57	98·57	98·65	99·04	98·47	97·93	98·22	99·02	99·57	98·86	97·65	99·11	97·16	95·96	99·79
LOI	12·85	13·47	11·16	16·38	22·02	19·20	15·93	12·19	10·44	11·00	13·71	19·29	29·99	20·82	10·85
$^{87}Sr/^{86}Sr$	0·708805	0·708904	0·706780	0·706355	0·708819	0·705195	0·707263	0·715691	0·719196	—	0·710018	0·707954	0·709286	0·710045	—
$^{143}Nd/^{144}Nd$	0·512473	—	0·512675	0·512810	0·512373	0·512940	—	0·512217	0·512188	—	—	0·512477	0·512394	0·512377	0·512349
$^{206}Pb/^{204}Pb$	18·837	18·820	18·780	18·800	18·887	19·485	19·382	18·842	19·089	19·218	18·869	19·097	18·858	18·932	19·306
$^{207}Pb/^{204}Pb$	15·675	15·669	15·647	15·636	15·775	15·658	15·628	15·684	15·703	15·778	15·728	15·726	15·728	15·735	15·792
$^{208}Pb/^{204}Pb$	38·824	38·784	38·671	38·675	39·181	39·078	39·080	38·768	39·064	39·260	38·994	38·900	38·979	38·951	38·970
Li	51·6	59·5	47·5	60·6	—	—	—	51·5	52·9	39·5	66·5	54·4	—	—	34·8
Be	1·86	1·85	1·10	0·78	1·87	1·09	1·04	2·53	2·80	2·86	2·35	1·54	2·11	1·99	0·99
Sc	22·9	23·2	29·2	30·4	45·1	34·7	36·7	7·92	8·72	8·26	19·7	31·6	51·1	48·5	13·9
V	182	200	196	296	188	214	267	71·3	68·5	70·2	188	205	270	140	53·5
Cr	91·7	55·9	30·6	14·0	37·2	938	810	89·0	88·4	61·4	87·9	22·9	29·2	29·1	6·35
Co	47·6	50·9	38·7	29·3	431	76·3	62·8	6·49	3·69	10·8	74·0	110	419	298	54·1
Ni	86·6	59·3	31·0	17·2	591	374	409	20·1	16·5	54·9	116	93·8	557	633	135
Cu	133	115	106	118	—	—	—	19·0	14·7	28·0	155	199	—	—	247
Zn	130	110	—	102	—	—	—	280	87·8	—	—	155	—	—	114

Site:	204	204	204	204	204	204	204	275	275	275	596	596	596	596	596
Core:	1	1	1	3	5	6	9	1	2	4	1	2	2	3	6
Section:	1	3	4	2	5	2	3	1	3	2	1	3	6	6	6
Interval (cm):	30–33	52–55	103–106	103–106	60–63	66–69	67–70	113–116	55–60	10–15	115–118	85–88	77–80	84–87	124–127
Depth (m):	0.3	3.52	5.53	50.53	100.60	105.16	144.67	1.13	8.57	35.10	1.15	9.35	13.77	23.44	48.54
Unit:	1	1	1	1	1	2	3	1	1	2	1	1	2	2	3B
Ga	19.9	20.8	18.4	15.9	22.8	17.3	18.6	11.2	11.6	13.9	20.7	16.1	19.5	20.0	5.68
Rb	88.2	91.7	48.1	31.2	72.8	65.3	21.5	132	146	129	116	59.3	58.7	75.9	16.7
Sr	242	221	204	150	306	212	87.5	179	100	74.4	237	220	387	247	147
Y	43.3	39.6	34.1	40.3	260	227	21.7	21.5	20.7	29.4	43.1	78.1	489	301	104
Zr	107	112	86.7	91.3	197	174	158	117	111	130	123	134	244	183	86.0
Nb	9.73	9.19	4.46	2.38	18.4	27.3	25.2	11.3	12.5	16.7	12.9	6.85	18.8	10.7	4.49
Cs	5.51	5.84	2.93	1.67	5.52	0.699	0.259	9.29	10.3	11.3	7.38	3.12	5.32	5.78	0.746
Ba	558	563	441	119	608	145	337	630	448	872	478	271	411	644	290
La	24.8	22.8	11.9	10.2	168	16.8	15.0	24.7	24.6	31.2	28.3	31.6	300	187	59.9
Ce	53.9	58.3	30.6	25.5	456	39.2	35.2	47.1	49.1	69.2	73.8	63.6	492	346	74.0
Pr	6.89	6.46	3.73	3.42	52.4	5.69	5.06	5.74	5.96	8.27	7.77	8.86	86.4	55.6	16.7
Nd	28.5	26.5	16.5	16.1	206	23.4	20.8	21.2	22.1	31.2	31.4	38.5	343	220	70.8
Sm	6.70	6.32	4.34	4.61	44.5	5.41	4.84	4.70	4.32	6.15	7.17	9.60	72.3	47.8	15.8
Eu	1.59	1.50	1.20	1.31	10.9	1.86	1.75	0.707	0.695	0.990	1.63	2.44	17.6	11.8	3.60
Gd	6.87	6.48	4.94	5.35	48.4	5.80	5.40	3.94	3.73	5.41	7.24	10.8	81.2	52.8	16.3
Tb	1.07	0.987	0.793	0.924	6.70	0.808	0.758	0.527	0.526	0.764	1.08	1.73	11.4	7.55	2.43
Dy	6.56	6.10	5.06	6.00	39.6	4.62	4.34	3.09	3.05	4.35	6.50	10.9	69.1	45.4	14.5
Ho	1.37	1.27	1.10	1.31	8.16	0.839	0.787	0.632	0.617	0.874	1.34	2.32	14.6	9.44	2.99
Er	3.90	3.65	3.11	3.79	23.0	2.29	2.11	1.84	1.77	2.46	3.75	6.56	41.0	26.5	8.17
Tm	0.572	0.533	0.476	0.576	2.85	0.296	0.283	0.274	0.264	0.359	0.555	0.975	5.06	3.35	1.16
Yb	3.64	3.42	3.11	3.49	17.9	1.78	1.70	1.75	1.72	2.29	3.56	6.23	31.5	21.3	7.25
Lu	0.548	0.516	0.465	0.572	2.72	0.260	0.242	0.257	0.257	0.345	0.542	0.952	4.84	3.27	1.09
Hf	2.67	2.80	2.23	2.33	5.42	4.17	3.99	3.26	3.04	3.43	2.81	3.41	6.24	4.88	1.70
Ta	0.62	0.59	0.27	0.14	0.91	1.66	1.57	0.96	1.06	1.48	0.77	0.371	0.70	0.52	0.22
Pb	30.5	35.3	18.7	9.86	65.8	1.35	1.16	19.2	13.1	11.7	49.4	91.1	89.0	99.0	55.2
Th	7.88	8.83	3.91	1.74	18.2	1.69	1.50	9.09	10.6	12.0	10.2	4.72	18.1	8.92	1.88
U	1.51	1.51	0.793	0.682	1.57	1.22	0.511	2.80	2.75	9.33	1.84	1.84	3.20	1.34	2.10

Abundances recalculated to anhydrous basis. Total Fe analysed as Fe_2O_3.
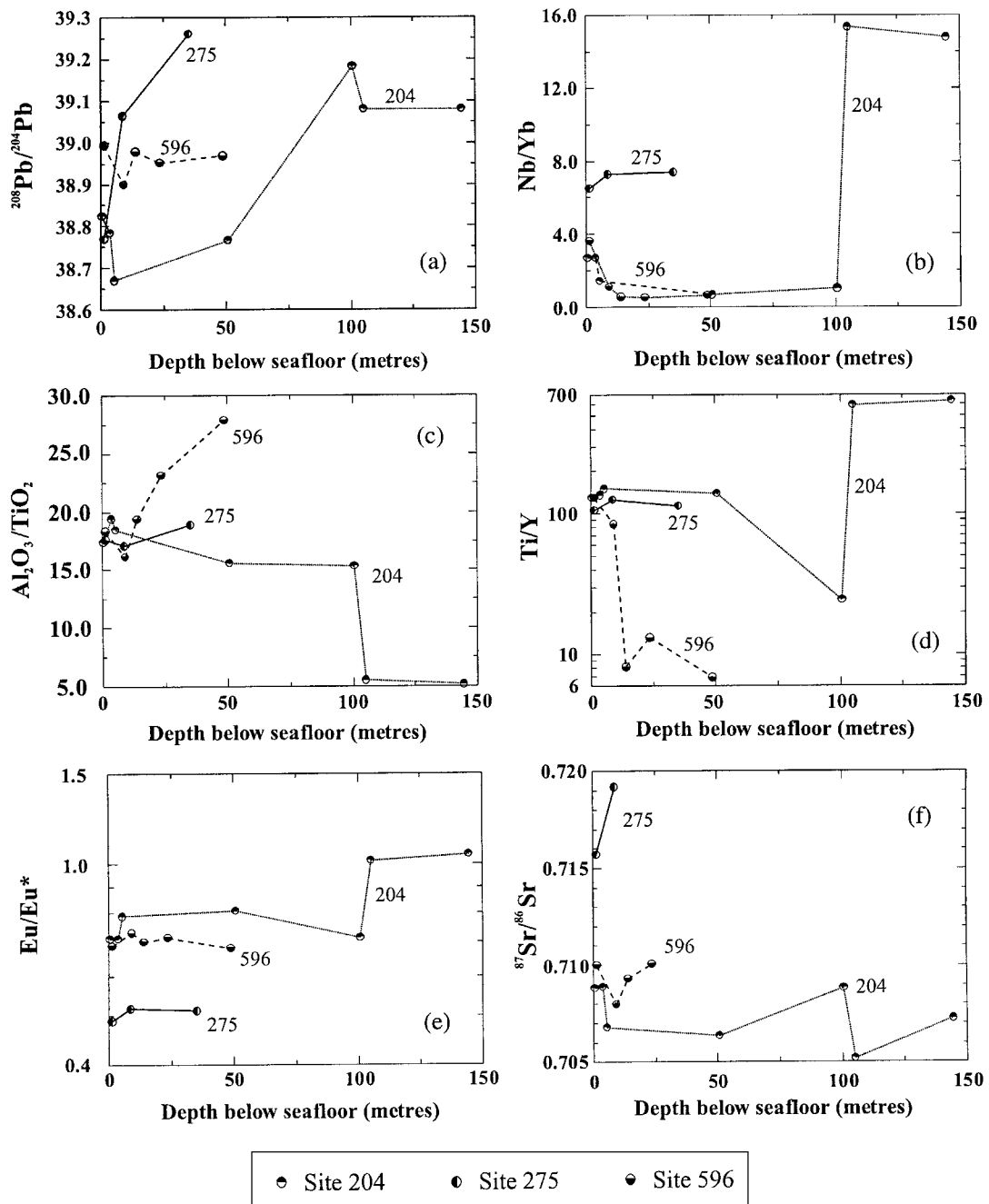
Fig. 2. Selected isotopic and elemental ratios plotted as a function of depth, for DSDP Sites 204 and 275, and ODP Site 596.

seawater compositions), the ratios are mostly below those of seawater in the sediments at Sites 204 and 596.

The geochemical variations with depth at Site 204 (excluding the LR-SMC-derived Units 2 and 3) largely reflect the increasing ash influence from the arc as the Pacific Plate has moved towards the arc; this is especially illustrated by Pb isotopes (Fig. 2a), which become less radiogenic with decreasing depth, and contrasts with the more uniform Pb isotopic compositions of sediments from Site 596, situated further from the arc.

THE MANTLE WEDGE COMPOSITION—REGIONAL GEOCHEMICAL PATTERNS

Introduction

Previous geochemical studies of lavas from the Tonga–Kermadec arc (Ewart & Hawkesworth, 1987; Ewart *et al.*, 1994*a*) have documented the pronounced HFSE depletion and LILE enrichment, relative to N-MORB (normal mid-ocean ridge basalt), features also, to differing degrees, of lavas from other oceanic arcs (Pearce & Parkinson, 1993; Woodhead *et al.*, 1993). Although variations of these depletion or enrichment patterns in Lau–Tonga–Kermadec lavas have been interpreted as resulting from two separate petrogenetic processes (e.g. Woodhead *et al.*, 1993; Ewart *et al.*, 1994*a*), comparable intra-arc variations within the South Sandwich Islands have been interpreted as reflecting dynamic melting processes within the sub-arc mantle wedge (Pearce *et al.*, 1995).

Results from ODP Leg 135 (Hawkins *et al.*, 1994) have documented the transitions of geochemistry and petrology that occur within the Lau Basin. In the older, western Lau Basin (e.g. Site 834), lavas with N-MORB geochemical characteristics are intercalated with lavas having arc-like chemistry, whereas in the eastern Lau Basin, closer to the modern arc, the lavas have an increasingly arc-like geochemistry. Although this trend is interrupted by the younger, propagator-driven spreading in the central–eastern Lau Basin, the increase in arc-like geochemical characteristics is also observed in the ELSC-VF propagator as it approaches the arc at its southern end (Vallier *et al.*, 1985; Jenner *et al.*, 1987; Boespflug *et al.*, 1990; Loock *et al.*, 1990; Fig. 1). These regional patterns of variation must, however, be viewed in relation to the changing geometry of the evolving arc–back-arc system. For instance, when erupted, the Lau Ridge and western Lau Basin lavas were much closer to the active arc than is now the case. It is therefore important to ascertain whether the geochemical variations are simply correlated with distance from the arc, or whether there is an additional temporal evolution of geochemistry, noting the age range of the back-arc lavas from ~6·5 Ma to present, and the older ages of much of the Lau Ridge arc volcanism.

Back-arc to arc transition

Comparison of back-arc and arc lavas is shown (Fig. 3a–d) using data normalized to 6% MgO. Ti is an element believed minimally modified by subduction processes (see later), and the fractionation-corrected Ti concentrations should therefore provide an indicator of the extent of source depletion. Figure 3 shows clearly the progressively decreasing Ti from back-arc to arc. Additional points illustrated by Fig. 3 are:

(1) The Tongan lavas, including the northern Tongan boninites, extend to lower Ti abundances than Kermadec lavas.

(2) The ODP Site 839 ('proto-Tonga' arc) lavas have higher Ti concentrations than most of the modern Tongan lavas.

(3) The LVG and KVG (the older Lau Ridge volcanic arc phases) are more Ti rich than the modern Tonga lavas. This is also true for the older, Tongan Ridge basement lavas.

(4) The Lau Basin lavas (both 'older' and 'new' groups), and the Niua fo'ou lavas are more titaniferous than the arc lavas.

(5) The Samoan, LR-SMC, and MVG OIB-type lavas are all significantly Ti enriched relative to the Lau Basin and the arc lavas.

Differences between arc and back-arc lavas are also seen in Na_2O contents (Fig. 3a) in which the arc lavas are depleted relative to the back-arc lavas, whereas 'subduction index' ratios (discussed more fully in a later section) such as Zr/Ba, Ce/Pb, and Nb/Th (Fig. 3b–d) show that those arc lavas most depleted in Ti tend to have the most arc-like chemistry. The ODP Site 839, LVG, KVG, older Tongan Ridge, and the VF lavas are intermediate between the modern arc and back-arc lavas. The 'depletion-index' ratios, such as Zr/Sm and Zr/Hf (Fig. 3e and f; Ewart *et al.*, 1994*a*), also indicate more depleted mantle beneath the arc than the back-arc. In the case of Zr/Hf, values decrease from about 40–45 in the least depleted back-arc lavas (including also the Samoa, LR-SMC, and MVG data), to <30 in the arc. In both plots, the Site 839 and VF lavas tend to have intermediate values, as do the data for the old Tongan Ridge and the Lau Ridge arc lavas.

Pearce *et al.* (1995) showed that in plots of Nb/Yb vs Th/Yb (and related plots), the lavas from the South Sandwich island arc define a linear array with positive slope. This was interpreted by Pearce *et al.* (1995) to reflect depletion of the mantle wedge during back-arc melting, followed by constant subduction input and dynamic melting to produce the arc lavas, the latter process inferred to control the range in Nb/Yb ratios. In the Tonga–Kermadec–Lau system (Fig. 4), the transitional behaviour between the Lau Basin and modern arc lavas is again particularly clear (Fig. 4a). However, the various arc lavas (the Tonga, Kermadec, and Site 839 'proto-arc' lavas) do not define a simple linear array (Fig. 4), whereas the northern Tonga lavas extend to relatively high Nb/Yb values. This suggests that the processes involved in arc magmatism in the Tonga–Kermadec–Lau system are inherently more complex than in the South Sandwich island arc, and/or that the mantle source is more heterogeneous.
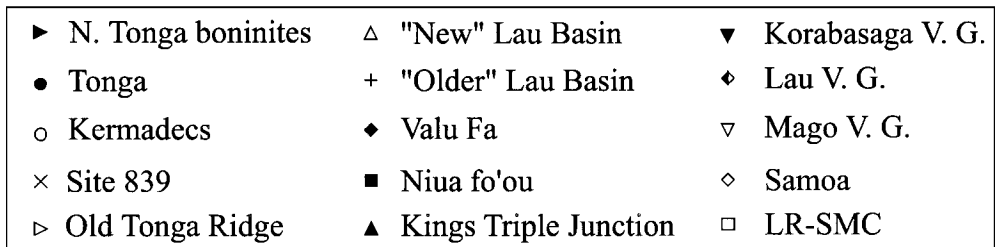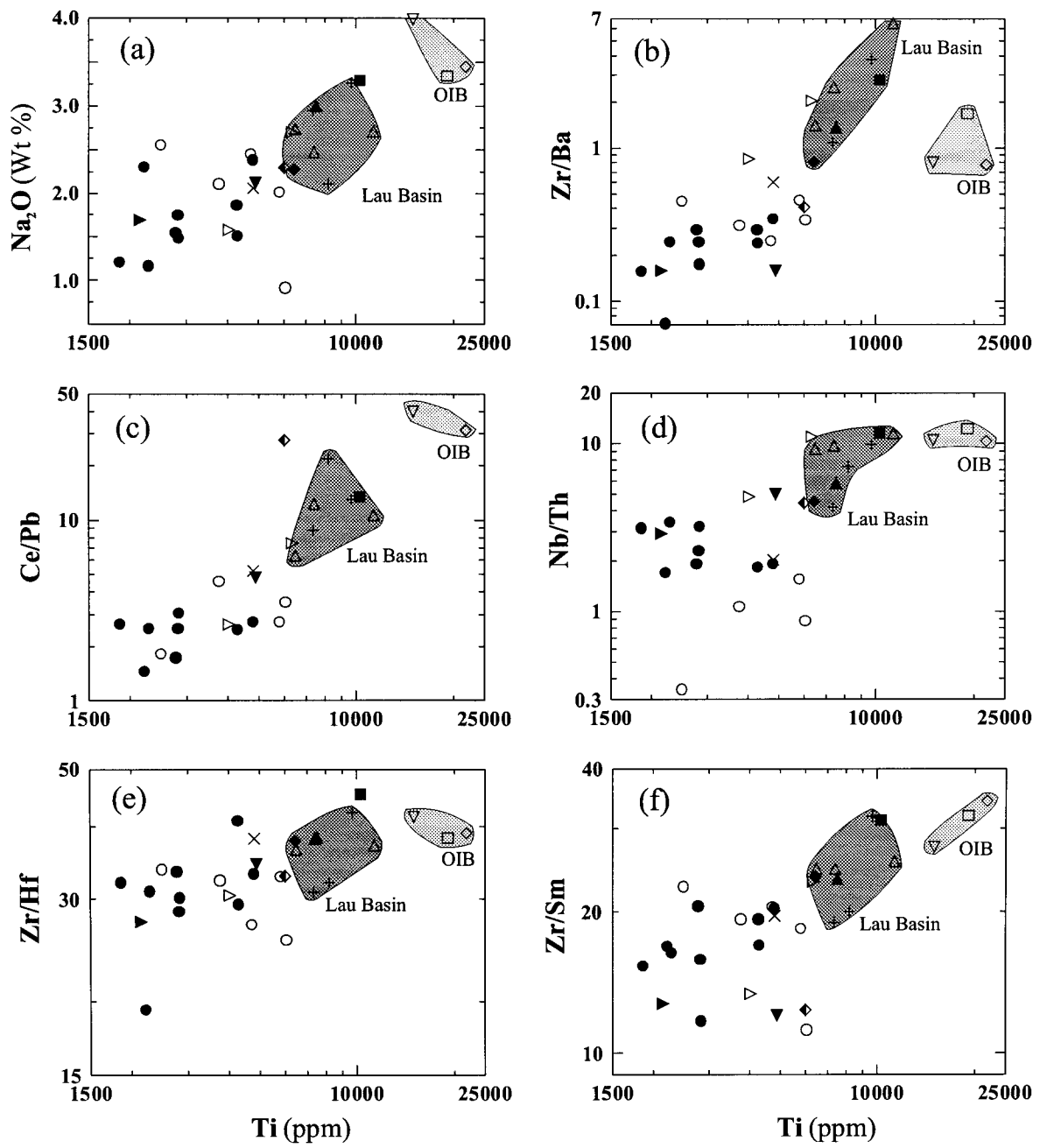
Fig. 3. Na_2O and selected element ratios plotted against Ti, a highly conservative element in the Tonga–Lau system. Plots based on data normalized to 6% MgO for each volcano and volcanic centre grouping (V.G.).
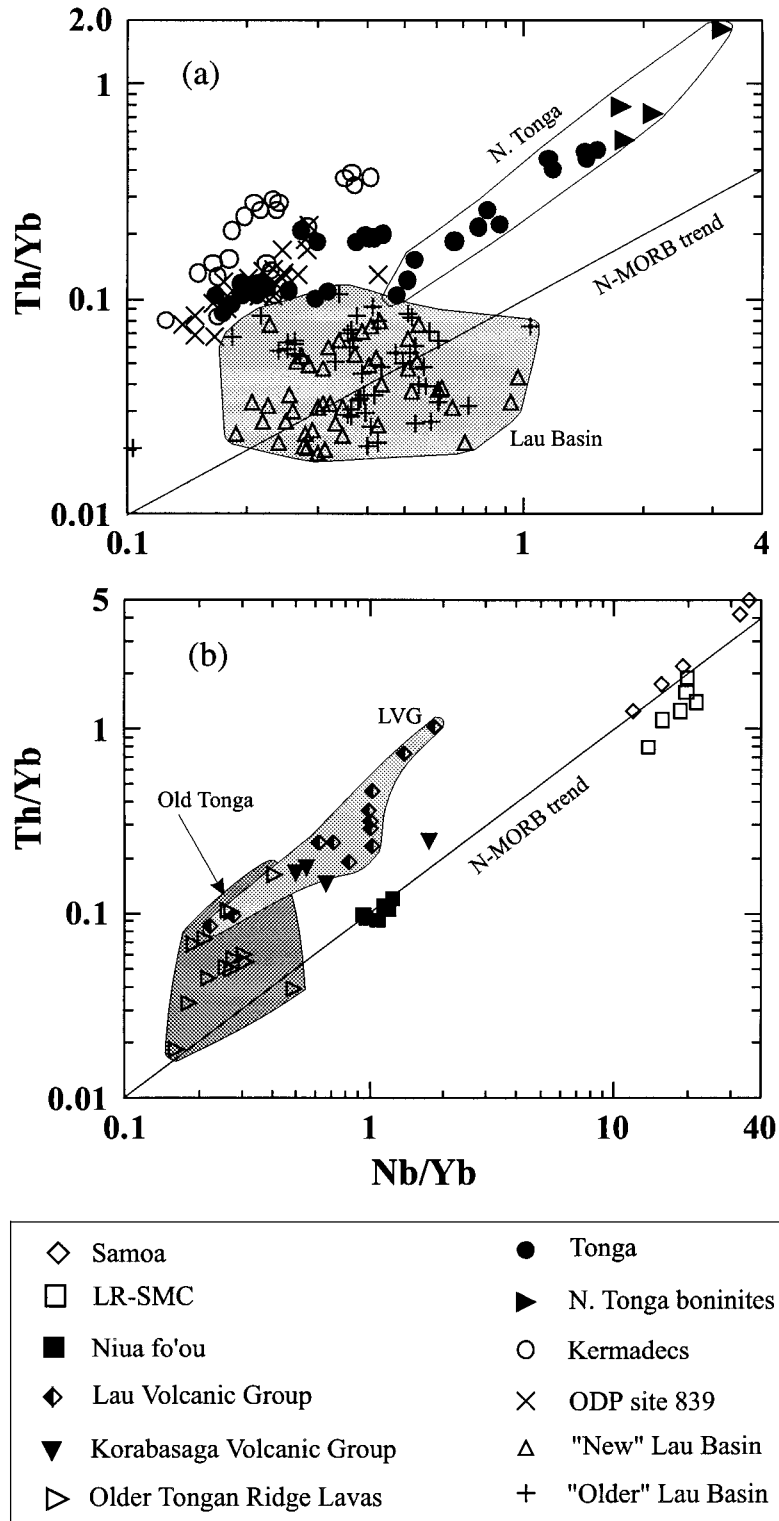
Fig. 4. Th/Yb vs Nb/Yb for (a) the modern arc, 'proto' Tongan arc (Site 839), and Lau Basin lavas, and (b) the older volcanic phases of the Lau Ridge, Niua fo'ou, Samoa, and the LR-SMC. N-MORB trend from Pearce *et al.* (1995).

Figure 4b compares the OIB compositions (Samoa and LR-SMC), Niua fo'ou, and the older volcanic phases of the Lau Ridge and Tongan Ridge. The LVG and KVG lavas have similar Th/Yb and Nb/Yb to the modern Tongan lavas, whereas the older Tongan Ridge lavas are similar to the Lau Basin lavas. The Niua fo'ou lavas lie on the N-MORB trend, but have higher Nb/Yb than the Lau Basin lavas, extending towards ratios characteristic of lavas from the LR-SMC and Samoa (discussed further in a later section).

In summary, the new trace element data for Tonga–Kermadec arc lavas confirm the transition from N-MORB-like to arc-like geochemistry from the back-arc to arc lavas, and also emphasize the distinctive chemistry of the arc lavas compared with the Samoan and LR-SMC OIB-type lavas. Niua fo'ou, although similar to the Lau Basin lavas, seems to exhibit a small shift towards OIB compositions. The new data generally confirm the intermediate chemistry, relative to the Lau Basin and modern arc, of the 'proto-Tongan' arc (ODP Site 839), the VF, and the older Lau Ridge volcanism (LVG, KVG), and Tongan Ridge basement lavas. The data therefore not only confirm the spatial geochemical changes between arc and back-arc, but further suggest that temporal changes of geochemistry have occurred within the arc lavas.

Latitudinal variation along the Tongan arc

Geochemical variation along the Tonga arc is evident in Pb, Sr and Nd isotopic compositions, certain trace element ratios, and HFSE and HREE (especially Ti, Yb, and Y) abundances. These show relatively systematic gradients, although sharp changes occur in Pb isotopic compositions, Nb/Yb and Zr/Ba ratios at the northern end of the Tonga arc. Some representative plots are illustrated in Fig. 5, with data from the Valu Fa Ridge and ODP Site 839 included for comparison. $^{87}Sr/^{86}Sr$ and Sc/Y increase, and $^{143}Nd/^{144}Nd$, Zr/Sm and Ti decrease northwards. The isotopic changes may reflect either changing subduction input compositions, or fluxes, and/or changing mantle wedge source compositions. The trace element data suggest a rather uniform subduction signature (Zr/Ba) except at the northern extremity of the arc, and a northerly increase in source depletion (Ti, Yb, and Zr/Sm), whereas the changing Sc/Y ratio is thought to reflect the changing balance between source depletion and enrichment (see below). The possible balance between rates of subduction and latitudinal changes of composition of subducted sediment or oceanic crust, is addressed below, but it is noted here that the available sediment data do not support the existence of latitudinal gradients of subducted sediment compositions along the Tonga arc, the most obvious divergence being evident

in the lowest two sediment units at DSDP Site 204, interpreted to be LR-SMC derived.

Indian and Pacific MORB source contributions to the arc melts

Hergt & Hawkesworth (1994) have argued that lavas erupted during the two phases of Lau Basin back-arc spreading ('older' and 'new' Lau Basin lavas) were derived from two different mantle domains, 'Pacific' and 'Indian' MORB mantle, respectively, which have distinct Pb isotope compositions. The new Pb isotope data show that Kermadec lavas lie close to the radiogenic end of the 'Indian' MORB array, whereas the Tongan lavas have less radiogenic compositions (Fig. 6a–d), with the least radiogenic samples having Pb isotope compositions approaching those of Pacific MORB. Lavas from the northern Tonga islands (Tafahi and Niuatoputapu) and the boninites are all isotopically different from other Tonga lavas, extending to higher $^{206}Pb/^{204}Pb$ ratios.

Pacific sediments have high Pb concentrations (Table 2), and during alteration of the oceanic crust, Pb is remobilized and concentrated in the upper part of the crust (Muhe et al., 1997). Pb is extremely soluble in hydrous fluids (Keppler, 1996), and thus the Pb contribution from the depleted upper mantle is likely to be small compared with the Pb derived from the subducting sediment and altered oceanic crust. Ce/Pb values of the modern arc lavas (average 2–3; Fig. 3c) compared with average MORB (~25) imply that ~80–90% of the Pb is derived from subducted material. The modern arc lavas define an array extending between Pacific MORB and Pacific sediment (Fig. 6), reflecting mixing between these two endmembers (Regelous et al., 1997). Further evidence that much of the Pb in Tonga lavas is derived from the subducting Pacific Plate is provided by the Pb isotope signatures of the subducting LR-SMC, which is seen in the arc lavas from northern Tonga (see below).

The ODP Site 839 lavas have 'Pacific' Pb isotopic affinities (Fig. 6a and b), consistent with addition of Pb during subduction before the second stage of Lau Basin opening. VF lavas have similar Pb isotope compositions to the southern–central Tonga lavas, perhaps reflecting the proximity of the VF to the modern subduction zone. The 'Indian' Pb isotope signature of the 'new' Lau Basin lavas may simply reflect upwelling of fresh upper mantle, unmodified by subduction, in response to crustal extension in the back-arc.

On Sr–Nd and Sr–Pb isotope plots (Fig. 7b and c), the 'older' Lau lavas have 'Pacific'-like compositions. In contrast, 'new' Lau Basin lava compositions overlap those of southern–central Tongan arc lavas, and both have relatively high $^{87}Sr/^{86}Sr$ ratios compared with Indian or Pacific MORB. The LVG (Lau Ridge) and the Tongan
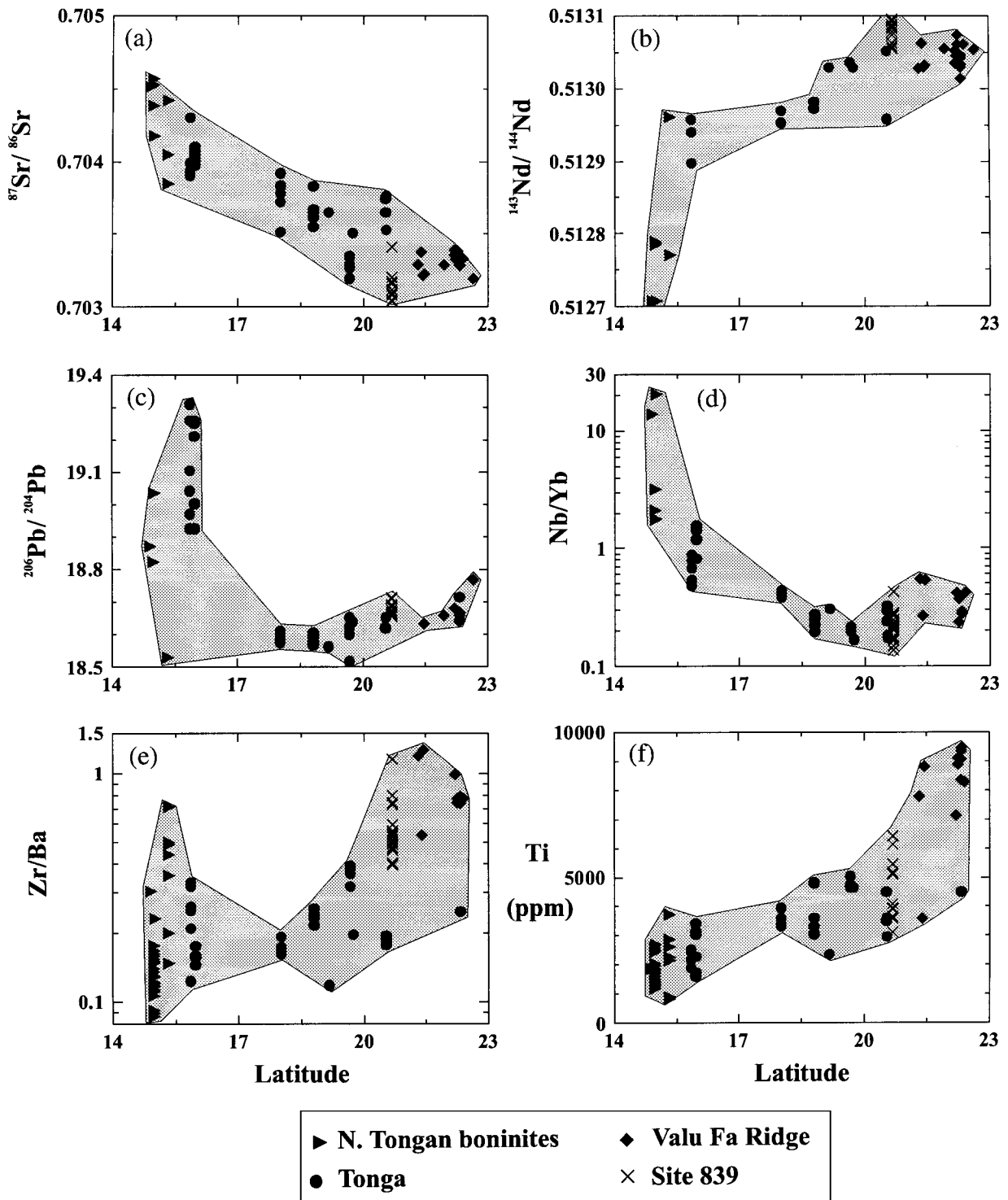
Fig. 5. Latitudinal (°S) geochemical changes along the Tongan arc, including 'proto' Tongan arc (ODP Site 839) and Valu Fa Ridge.
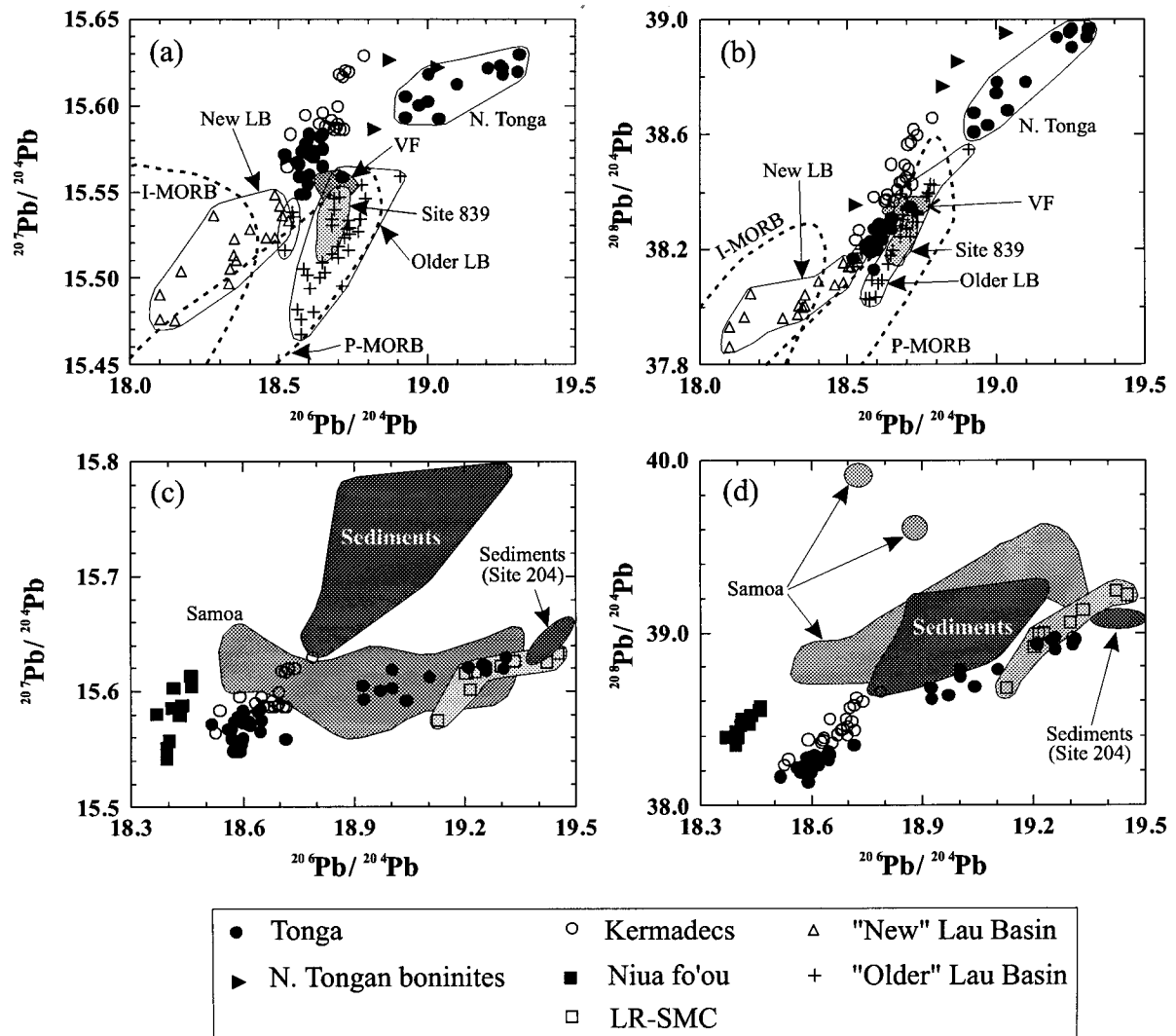
Fig. 6. Pb isotope plots for: (a) and (b), the Lau Basin, Valu Fa (VF), Site 839, and modern Tonga–Kermadec arc [Indian and Pacific MORB fields from Ferguson & Klein (1993)]; (c) and (d), modern Tonga–Kermadec arc compared with Niua fo'ou, Samoa, LR-SMC, and sediments from DSDP Sites 204 and 275, and ODP Site 596. The separate Site 204 sediment field refers specifically to Units 2 and 3.

'proto-arc' (Site 839) lavas overlap (Fig. 7e), with both having lower Sr and higher Nd isotopic ratios than the modern Tonga–Kermadec lavas, and thus closer to the 'old' Lau Basin lavas ('Pacific' MORB source). The younger KVG (Lau Ridge), however, extend to more radiogenic Sr and less radiogenic Nd, thereby overlapping the modern arc lavas. Although this can be interpreted as increasing 'Indian' MORB source influence, it may additionally reflect increased subduction input. Direct comparison of Sr and Nd isotope compositions, however, may be complicated by the decoupled behaviour of Sr and Nd in subduction zone processes (see below). The northern Tongan arc lavas and boninites have Sr and

Nd isotope compositions similar to Samoan and LR-SMC lavas.

Influence of the Samoan plume in northern Tonga

Lavas from the northern Tongan volcanoes of Tafahi and Niuatoputapu, and the boninites (Danyushevsky *et al.*, 1995) from the extreme northern termination of the arc, are clearly displaced towards the Samoan and LR-SMC arrays from the main Tongan compositions, in plots incorporating Nb (Figs 4a and 8a–c). This is also
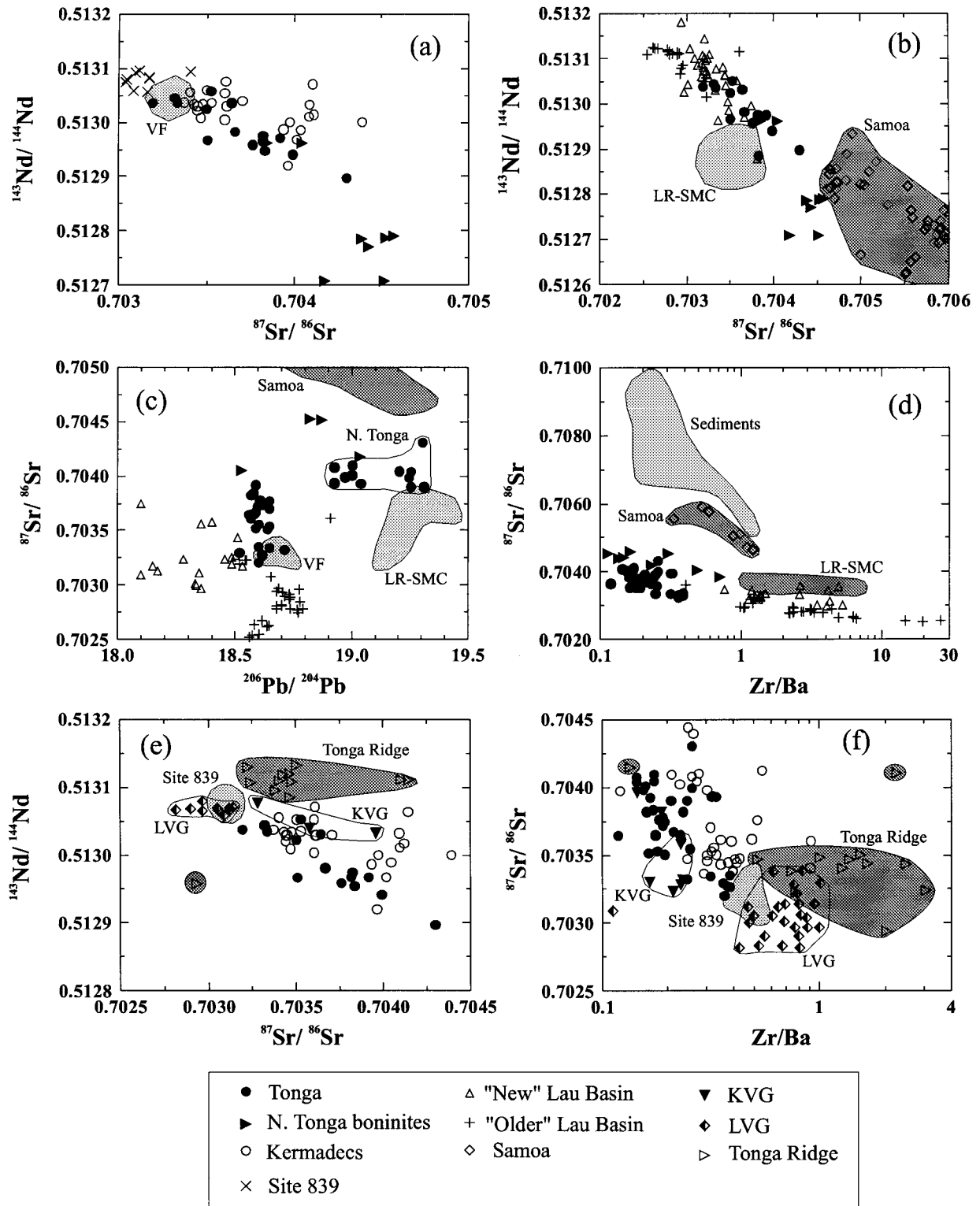
Fig. 7. $^{87}Sr/^{86}Sr-^{143}Nd/^{144}Nd$, $^{87}Sr/^{86}Sr-^{206}Pb/^{204}Pb$, and $^{87}Sr/^{86}Sr-Zr/Ba$ relations. (a)–(d), modern Tonga–Kermadec arc, Lau Basin, VF, Site 839, LR-SMC, Samoa, and sediments (Sites 204, 275 and 596). (e) and (f), the modern arc, Site 839, and the older, arc-like lavas from the Lau Ridge and Tonga Ridge.

characteristic of lavas from Niua fo'ou, relative to other Lau Basin lavas. Wendt *et al.* (1997) have attributed the relatively high Nb in lavas from northern Tonga and Niua fo'ou to the presence of an OIB component derived from the Samoan plume in the upper mantle beneath the northern Lau Basin and Tonga arc (see also Volpe *et al.*, 1988). OIB lavas have high concentrations of Nb relative to other HFSE (e.g. Zr, Figs 4a and 8a–c) compared with MORB or arc lavas. The critical point is that the Samoan plume input into the arc lavas is inferred to occur by direct flow of asthenosphere south-wards beneath the northern end of the Tonga arc and Lau Basin, and is therefore independent of subduction processes. As a result, the Samoan plume signature cannot be detected in the isotopic compositions of Sr and Pb in the arc lavas, these elements being derived dominantly from the subducting slab, rather than the depleted mantle wedge (see later). An additional aspect is that within the northern Lau Basin, the OIB signature appears to be restricted to lavas that are younger than ~5 Ma, reflecting relatively recent influx of Samoan OIB mantle across the boundary between the Pacific and Indian Plates at the northern end of the Tonga arc (Wendt *et al.*, 1997).

Niua fo'ou

Lavas from the subaerial active back-arc volcano of Niua fo'ou are chemically and mineralogically distinct from the arc volcanoes (e.g. Ewart *et al.*, 1977, 1994*a*), and have trace element affinities with the Lau Basin lavas of N-MORB type (Reay *et al.*, 1974). The new data show that Niua fo'ou is, relative to the Lau Basin floor lavas, enriched in CO_2 and F (comparable with the arc lavas, Fig. 9), whereas in element ratio plots, its compositions lie at the 'enriched' end of the Lau Basin arrays, consistent with minimal subduction input (Fig. 3). Relatively high Nb concentrations, however, suggest possible Samoan plume input (Fig. 4). Niua fo'ou lavas are relatively enriched in Ti (Fig. 3) and Y, comparable with the 'least' depleted Lau Basin basaltic lavas, but are not as enriched as the MVG, Samoa, or LR-SMC lavas. The new trace element data therefore support the affinity of Niua fo'ou to the N-MORB-like Lau Basin back-arc lavas, but containing a relatively small OIB component.

Sr, Nd and Pb isotopes, however, show no clear similarities to any of the Lau Basin, OIB, or arc lavas or sediments. One possible scenario seems to be mixing between 'Indian' Lau Basin MORB mantle and a subset of the Samoan lavas (post-erosional lavas), but even this is not entirely consistent with $^{207}Pb/^{204}Pb$–$^{206}Pb/^{204}Pb$ compositions (Fig. 6). Such mixing is feasible given the geographic position of Niua fo'ou in Northern Lau Basin and the Nb 'anomalies' discussed above. That Niua fo'ou is the only subaerial central volcano within the Lau Basin

suggests that it may emanate from a localized plume within the Lau Basin asthenosphere, perhaps initiated by instabilities caused from the postulated inflow of asthenosphere from the north into the opening Lau Basin (Giardini & Woodhouse, 1986).

ISOTOPE–TRACE ELEMENT CORRELATIONS: THE SUBDUCTION INPUT

Introduction

Element ratio plots of the Lau–Tonga–Kermadec lavas commonly show linear trends suggestive of mixing, especially when 'non-conservative' elements (e.g. Cs, K, Rb, U) and more 'conservative' elements (e.g. Nb, Zr, Yb, Hf, Y) are compared. Relevant plots for the arc and back-arc data (Fig. 9) define nearly linear arrays (noting the small differences between 'older' and 'new' Lau Basin lavas), indicative of mixing relationships. The arc data lie at the Cs-enriched end of the arrays; the ODP Site 839, VF, and the Lau Basin back-arc lavas are progressively less Cs enriched. Samoa and LR-SMC lavas define separate arrays in each plot. Superimposed sediment data, although broadly defining the high-Cs termination of the arc arrays, are not consistent with simple bulk sediment mixing into the arc melts or sources. This is considered to reflect the decoupled behaviour of Cs and HFSE in subduction fluids; the arrays in Fig. 9 have slopes of ~1, consistent with addition of Cs, but not Zr, Nb, Yb or Y from the subducting slab to the mantle wedge. Figure 9b and c clearly distinguishes the Site 204 LR-SMC-derived sediments (Units 2 and 3) from the other sediments. A further point illustrated by Fig. 9b and c is the shift of the northern Tongan data towards the Samoa array.

Sr–Nd isotopic compositions (Fig. 7a and b) exhibit transitional changes from 'older' and 'new' Lau Basin, through ODP Site 839 and VF, to the modern arc data arrays (noting the trends of the boninitic suite towards the Samoan compositions). These isotopic shifts are interpreted to result from increasing subduction input, involving a more radiogenic Sr and less radiogenic Nd endmember. Pb isotopic compositions of the southern–central Tonga and Kermadec arc lavas lie between the Pacific MORB and sediment compositions (Figs 6c and d). This is interpreted to reflect mixing of Pb from two major sources; subducted Pacific Ocean crust and subducted sediment as discussed above, with Kermadec lavas containing a larger sediment contribution. The shift in Sr isotopes is correlated with certain element ratios, most notably Zr/Ba (Fig. 7d), which is a good indicator of slab flux as a result of the different behaviour of the two elements in subduction zone processes. Although
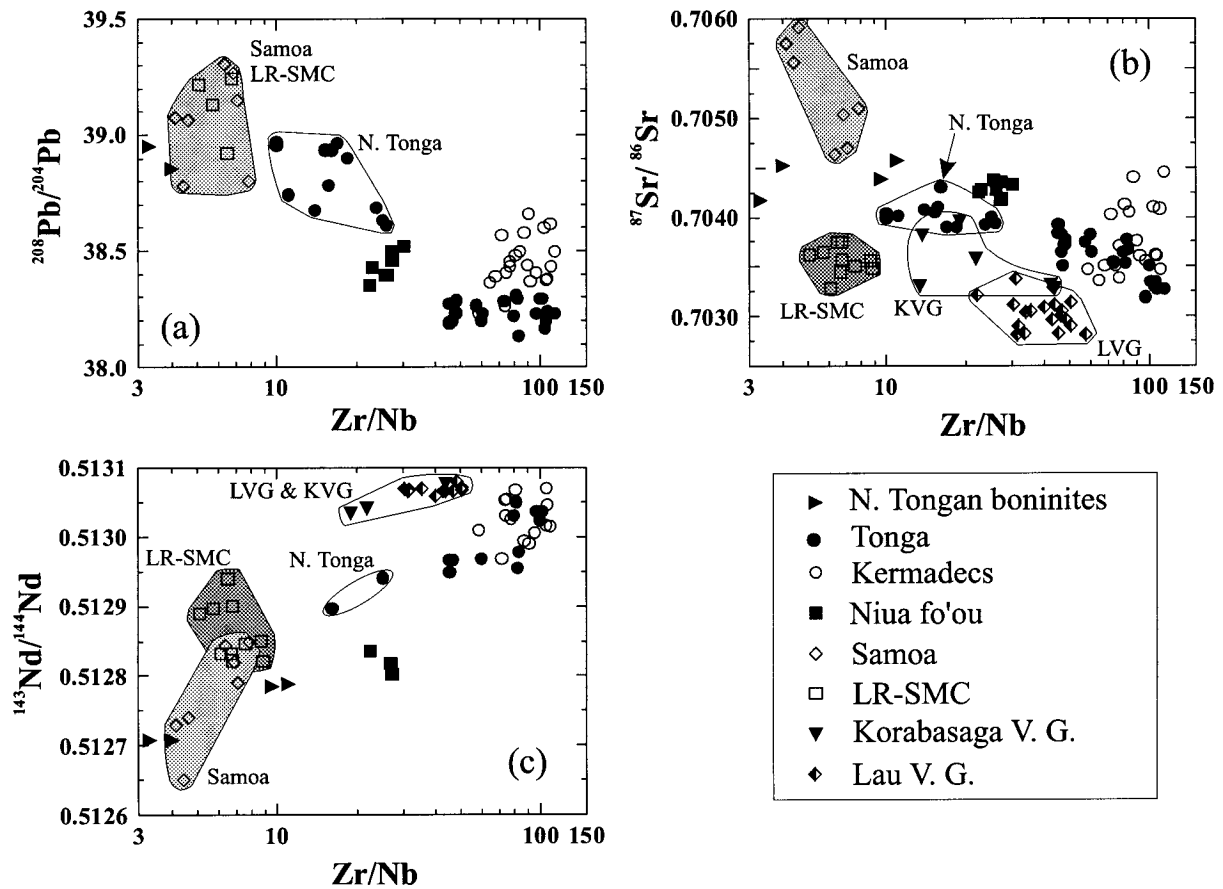
Fig. 8. Pb, Sr, and Nd isotopic compositions vs Zr/Nb ratios of modern arc lavas, older arc-like Lau Ridge volcanic phases, Samoa and LR-SMC.

$^{87}Sr/^{86}Sr$ and Zr/Ba are negatively correlated in the arc and back-arc lavas, the data again imply that simple bulk mixing with sediment cannot explain the trends, reflecting decoupling of the various elements during addition of subduction fluid to the mantle wedge (see below). The data also show that bulk mixing of Samoan plume mantle into a subduction modified mantle wedge cannot explain the observed compositional variations.

Volatile abundances

Analyses of F, CO_2 and H_2O have been made on a subset of arc and back-arc samples (Appendix), based on the inference that addition of the subduction-derived component to the mantle wedge will result in positive correlations between volatile concentrations and subduction-controlled trace element and isotopic signatures (e.g. Stolper & Newman, 1994). The analysed back-arc lavas, all vesicular, were drilled from water depths >2 km, whereas all arc samples, although non-vesicular,

were erupted subaerially. The H_2O, F, and CO_2 plots (Fig. 10) broadly distinguish the back-arc, proto-arc (ODP Site 839), and modern arc fields, with the proto-arc data apparently showing slightly lower volatile abundances than the modern arc lavas.

The increase in both CO_2 and F in the arc lavas seems puzzling in view of expected subaerial degassing effects. If CO_2 and F loss has occurred, then differences between pre-degassed arc and back-arc magmatic lavas would have been even more pronounced. In the case of H_2O, the arc lavas are much lower than back-arc samples, presumably reflecting low-pressure H_2O loss. H_2O abundance levels in the proto-arc and back-arc lavas range between 0·49 and 1·96% (excluding samples in which secondary hydration has clearly occurred), and between 0·68 and 1·96% for quenched glasses. These compare with the corresponding range of 0·33–1·08% for the arc lavas. CO_2 and F abundances for Niua fo'ou are comparable with the arc lavas. Macpherson & Mattey (1994) reported CO_2 concentrations of 94–217 ppm for
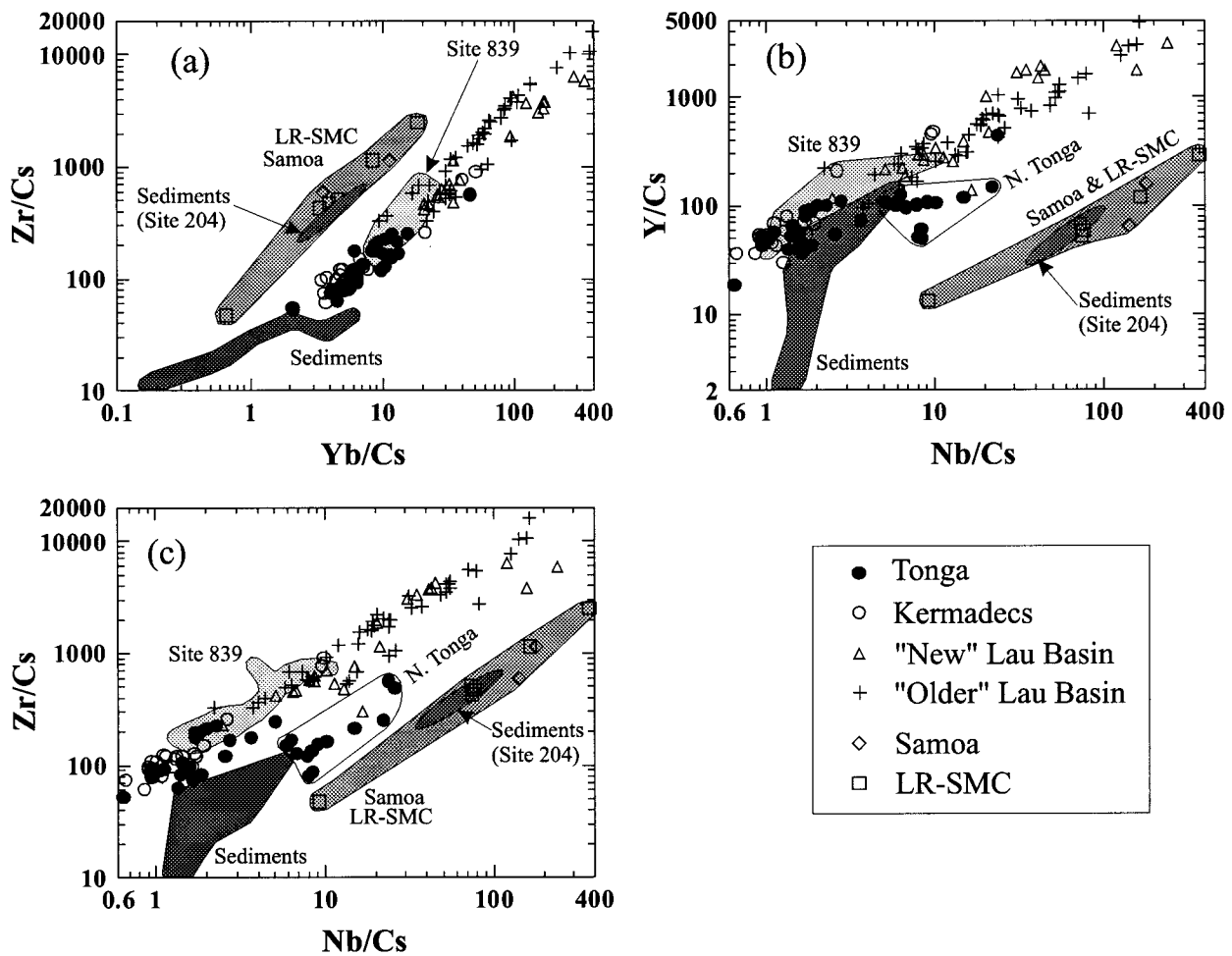
Fig. 9. Zr/Cs, Yb/Cs, Nb/Cs and Y/Cs ratio plots comparing modern Tonga–Kermadec arc and Lau Basin, Samoa, LR-SMC and sediments (DSDP Sites 204 and 275, and ODP Site 596). Sediment labelled from Site 204 refers specifically to Units 2 and 3.

ELSC and ILSC samples, which compare with our values of 210–240 ppm from ODP Site 836 (our nearest comparison with the analysed ELSC-ILSC samples).

The data of Dixon & Stolper (1995) on vapour-saturated basalts, at constant pressure, show that inverse correlations between CO_2 and H_2O (at 1200°C) are expected. Comparison, however, of our data with the calculated equilibrium curves (Fig. 10a) suggests that equilibration is more consistent with pressures between 400 and 800 bars, significantly higher than the water depths (2–4 km) in which the back-arc samples were recovered (and which are likely to have been even less during their eruption; Parson et al., 1992). This suggests that back-arc magmas were volatile supersaturated. The problems posed by the volatile abundances of the arc lavas are emphasized by the expected degassing behaviour (Dixon & Stolper, 1995) in which CO_2 is strongly

partitioned into the vapour phase during degassing and lost, whereas melt water contents remain relatively unchanged until near the surface. The arc volatile data therefore suggest significantly higher original melt CO_2 abundances than analysed, which is consistent, for example, with the data of Harris & Anderson (1984).

Additional complications are caused by fractional crystallization, which will enhance melt volatile levels (noting especially the wide range of *mg*-number of the arc and back-arc lavas), although preserving the negative correlation between CO_2 and H_2O (Dixon & Stolper, 1995; although this is also further complicated by polybaric fractionation). In fact, plots of *mg*-number vs volatiles (not shown) do exhibit positive correlations with F, H_2O, and CO_2 for the samples from the 'older' Lau Basin volcanic phase (*mg*-number 28–65), but not for the other sample subsets.
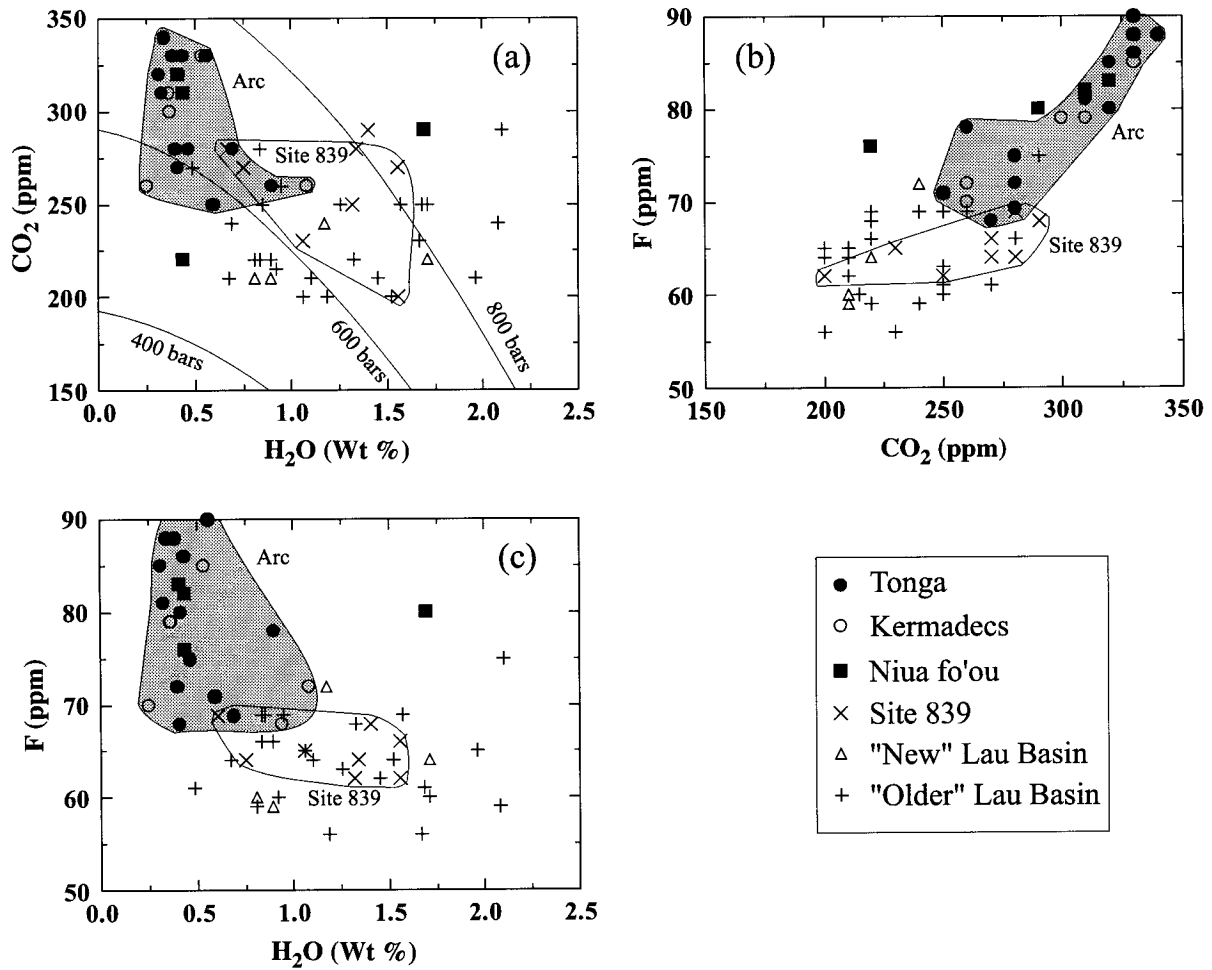
Fig. 10. Volatile abundances within the arc and back-arc lavas. In (a), the curves represent concentrations of H_2O and CO_2 in basaltic melts saturated with CO_2–H_2O vapour at the indicated pressures, after Dixon & Stolper (1995).

In summary, the volatile contents of the arc and back-arc lavas are believed to reflect: (1) higher primary CO_2 and F ($\pm H_2O$?) contents of the arc lavas compared with the back-arc melts, the analysed values for the arc lavas representing minimum values for the arc magmas before eruptive degassing; (2) polybaric degassing within the back-arc lavas, expected in view of their range of ages and locations; (3) effects of fractional crystallization, best seen in the 'older' Lau Basin data; (4) the relatively high CO_2 and F contents, comparable with the arc lavas, in back-arc lavas from Niua fo'ou.

Comparison between the Tongan and Kermadec Arc segments

As shown, geochemical variation occurs in the lavas erupted along the Tongan arc, and Gamble *et al.* (1996) have demonstrated the existence of Pb isotope compositional gradients along the Kermadec arc. Although these variations complicate direct comparisons between the two arc segments, isotopic and trace element abundance patterns do show differences. A key difference is the Th/U ratio (Fig. 11c), but the Kermadec lavas also tend towards higher Ti, Ce/Pb and Zr/Ba (Figs 3, 7 and 11). Average Th/U ratios are 2·22 ($\sigma = 0·57$) for Kermadec lavas, compared with 1·63 ($\sigma = 0·78$) for Tonga.

Isotopically, the two arc segments also define distinct fields, most notably in Pb isotope space (Figs 6 and 11), in which the Kermadec and Tongan data show only minor overlap. When viewed in the perspective of the regional isotopic and trace element data arrays, including the sediments and the Samoan and LR-SMC data (Figs 6 and 11), the following points emerge:

(1) The Kermadec Pb isotope data project closer to, and overlap the sediment data (excepting the samples from Site 204 Units 2 and 3), relative to Tonga.
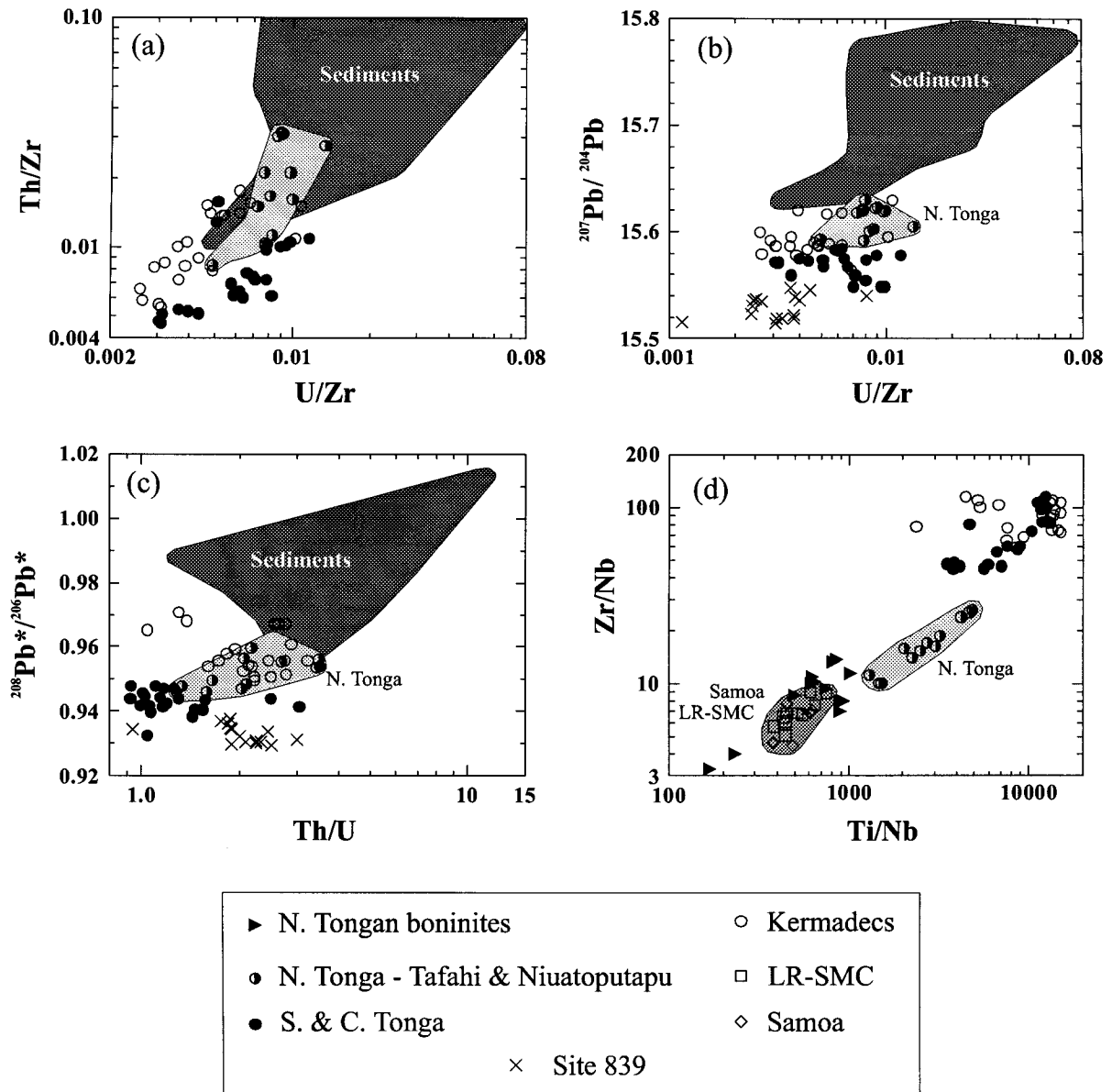
Fig. 11. Comparison of selected element ratios, ^{207}Pb/^{204}Pb, and radiogenic ^{208}Pb*/^{206}Pb*, of the Northern Tonga, southern–central Tonga, Site 839, and Kermadec arc lavas, compared with Samoa, LR-SMC, and sediments from DSDP Sites 204 and 275, and ODP Site 596.

(2) These relations extend to the ^{208}Pb*/^{206}Pb*–Th/U and Th/Zr–U/Zr relations (Fig. 11a and c), noting the higher ^{206}Pb/^{204}Pb of the northern Tonga (Tafahi and Niuatoputapu) lavas compared with other Tonga lavas (Fig. 5; see below). The differences in Th/Zr–U/Zr indicate differing slab components, whereas the positive array in Fig. 11c suggests that the Th/U differences between the two arc segments (Fig. 11a) are relatively long lived, consistent, for example, with a larger subducted sediment component in Kermadec lavas compared with Tonga lavas.

(3) As shown by Regelous *et al.* (1996, 1997) and Turner *et al.* (1997), lavas from the two arc segments also differ in U–Th disequilibrium systematics. Tonga lavas have high (^{238}U/^{232}Th) and (^{230}Th/^{232}Th) values (2·48–3·02 and 1·48–2·47, respectively) with all samples having excess U. In contrast, Kermadec lavas have lower (^{238}U/^{232}Th) and (^{230}Th/^{232}Th) values (1·09–1·52 and 0·84–

1·61), and are generally closer to equilibrium, with U excess or Th excess.

(4) The ODP Site 839 ('proto' Tonga arc) lavas have close trace element affinities with modern Tonga, although as previously noted, isotopic compositions are intermediate between the 'old' Lau Basin and modern Tongan arrays.

There is no evidence, therefore, that Tonga has evolved geochemically through a stage now represented by the Kermadec arc, and there is, instead, evidence for some fundamental difference between the Tonga and Kermadec arc segments.

Gamble *et al.* (1996) and Regelous *et al.* (1997) have concluded that the Kermadec arc sources are dominated by a sediment-related subduction input, which our data suggest has a significant continental derived component. In contrast, Regelous *et al.* (1996) have argued that the Tonga arc source is dominated by altered oceanic crust subduction. We believe, therefore, that it is the nature of the subduction components that results in the fundamental geochemical differences between the arc segments. Close to the Tonga Trench, the subducting Pacific Plate carries a relatively thin sediment cover (~200 m), whereas ~1 km thickness of sediment is being subducted at the Hikurangi Trench (Davey *et al.*, 1986). The migration of the LR-SMC southwards along the Tongan arc may also have played a role in these differences, by acting as a barrier to northward sediment movement parallel to the trench, and also possibly in removing forearc and trench sediment accumulations along the Tonga subduction zone.

The LR-SMC signature in northern Tonga

Lavas from the northern Tongan volcanoes of Tafahi and Niuatoputapu have Pb isotopic compositions which extend towards, and overlap the field for LR-SMC lavas, and the two sediment samples from Units 2 and 3 at Site 204 also have Pb isotope compositions similar to LR-SMC lavas, confirming their provenance (Fig. 6). Sr and Nd isotope data for Tafahi and Niuatoputapu lavas are also similar to LR-SMC samples (Fig. 7b and c), but in this case direct comparison may be misleading, as Sr and Nd may be decoupled during the subduction process. Trace element ratios of the northern Tonga lavas do not resemble those of LR-SMC lavas (Figs 9 and 10), except those using Nb, but as described, this reflects an OIB component derived from the Samoa plume (Figs 8, 9 and 11d). An additional feature shown by the two northern Tongan volcanoes is their heterogeneity with respect to Pb isotopes [this was noted by Ewart & Hawkesworth (1987), but attributed to possible sample contamination]. Leaching of samples and analyses of additional samples have now confirmed the isotopic heterogeneity of these

lavas, which suggests not only a heterogeneous mantle wedge source, but one that is presumably undergoing active mixing. The fact that lavas from the next most southerly active volcano (Fonualei), lying ~250 km south of Tafahi, do not show the LR-SMC isotopic signature suggests that Pb is taking some 2–3 my to travel from the subducted slab and back to the surface in lavas (Regelous *et al.*, 1996, 1997; Turner *et al.*, 1996). Following Wendt *et al.* (1997), we believe that Pb and Sr (plus other non-conservative elements) are transferred to the northern Tongan arc source via subduction fluids, hence the strongest LR-SMC signatures are evident in the Pb and Sr isotopic signatures.

THE SUBDUCTION BALANCE: ESTIMATION AND MODELLING

Introduction

Several factors complicate quantitative modelling of the subduction input to Tonga–Kermadec lavas: (1) the inferred north–south variation in the degree of depletion of the mantle wedge beneath the arc, and the presence of a Samoa OIB component in the mantle beneath the northernmost end of the Tonga arc; (2) the clockwise rotation of the Tongan ridge, resulting from the geometry of the second stage spreading within the Lau Basin, and leading to a northerly increase in the subduction rate (Jarrard, 1986; DeMets *et al.*, 1990); (3) variations in the amount and composition of material being subducted along the arc; less sediment in Tonga than in the Kermadec arc, and the LR-SMC beneath the northern end of the Tonga arc. Nevertheless, these processes, taken together, are believed to result in the observed latitudinal variations in the geochemistry of lavas erupted along the arc.

As discussed, the Samoan and LR-SMC geochemical signatures have been introduced into the northern Tonga arc lavas in very different ways (Regelous *et al.*, 1996; Wendt *et al.*, 1997). Southward flow of OIB mantle from the Samoa plume beneath the northern end of the Tonga arc results in high Nb, relative to other HFSE in northern Tonga lavas. In contrast, much of the Pb and Sr in these lavas is derived indirectly from the Louisville plume, by dehydration of plume-generated seamounts that were erupted onto the subducting Pacific Plate 80–90 my ago. The decoupling of conservative and non-conservative elements in the subduction zone allows the two plume contributions to be resolved. The relatively small sediment input into the Tonga Trench results in the 'Pacific-like' Pb isotope signature of southern and central Tonga lavas, and the LR-SMC Pb isotope signature of Tafahi and Niuatoputapu lavas.

Modelling

Three aspects of the modelling were undertaken, to test the effects of (1) mantle depletion on melt trace element geochemistry, (2) generalized subduction flux on arc melt geochemistry, here assumed to be imprinted on the melt source ('metasomatism') before melt separation, and (3) isotopic signatures of sediment vs oceanic crust subduction input.

Source depletion

Procedures follow those of Ewart & Hawkesworth (1987), extended by Pearce & Parkinson (1993). The model starting composition is spinel lherzolite corresponding to fertile MORB mantle (FMM; from Pearce & Parkinson, 1993). Comparison of the current data with the spinel and garnet lherzolite melting trends calculated by these workers favours the spinel model composition as the most relevant, as was also concluded by Pearce & Parkinson (1993) for intra-oceanic arcs with associated back-arc basins. Calculations utilized non-modal fractional melting (Shaw, 1970), with and without 'trapped liquid' treated as a separate phase (Pearce & Parkinson, 1993). In the graphs presented (Figs 12 and 13), the data are calculated without the 'trapped liquid', which we believe slightly better represents the analytical data. Rates of phase melting also follow Pearce & Parkinson (1993), i.e. clinopyroxene disappearing at 25%, and orthopyroxene at 40% melting. Details of the source mineralogy, and partition coefficients are given in Table 3. Progressive source depletion is calculated after 5, 10, 15, 20, and 25% prior fractional melting 'events' (referred to as RMM5 to RMM25, respectively), with appropriate adjustment of the phase mineralogy during the calculated melting steps; 1% porosity is assumed. Trace element compositions of the melts produced, by further fractional melting and pooling of melts of the RMM5 to RMM25 source compositions, are then calculated for 5, 10 and 15% remelting (i.e. second stage melts), believed to simulate the Tonga–Kermadec arc melt zones.

Subduction enrichment

To model the possible effects of subduction input, the composition of the subduction-derived 'H_2O-rich component', calculated by Stolper & Newman (1994) from the Marianas, is used. This has been derived independently of the Tonga–Kermadec data, and to a degree, avoids possible circular reasoning when comparing the calculated model results with the actual arc lava compositions, as would occur if Stolper & Newman's methods were applied specifically to the present data set. The RMM5 to RMM25 source compositions have therefore been modified by addition of 0·001, 0·005, and 0·01 weight fractions of the 'H_2O-rich component'. The second stage melting calculations are then repeated for 5, 10 and 15% melting, as before. The resulting curves (Fig. 12) for subduction modified source compositions are believed to approximate the effects of remelting of mantle wedge which has been modified by prior, variable melt extraction (i.e. source depletion) and then selective subduction-derived enrichment.

Trace element results

The analytical data presented for the arc and back-arc lavas in Fig. 12 are normalized to MgO = 6%. Comparison with the calculated curves suggests that only Yb and Ti are little modified by subduction input (i.e. are 'conservative'), with the Lau–Tonga data for these elements following the calculated trends for melts derived from progressively depleted mantle sources (Fig. 12a). In fact, the Lau Basin lavas extend to higher Ti and Yb than the model FMM composition, suggesting some to originate from source(s) slightly more enriched than 'typical' N-MORB source(s). The most 'enriched' lavas are the youngest ('Indian' type) Lau lavas, including Niua fo'ou.

All other elements modelled, when plotted against Yb, show varying degrees of departure from the calculated melt compositions from variably depleted sources. Examples specifically shown are Sm, Y, and Zr/Ba (Fig. 12b–d). Sm is an example, together with Zr and Nb, of moderate departures, and Y of stronger departures from the calculated depletion trends. In all cases, however, these 'departure' trends can be broadly matched with the calculated melt trends from the 'subduction modified' model sources containing between 0·001 and 0·005 'H_2O-rich component'. The relative success of the calculated curves in duplicating the observed data trends is exemplified by the Zr/Ba–Yb plot (Fig. 13d), even to reproducing subtle changes in slope within the observed arc and back-arc data.

The types of plots shown in Fig. 12, in which Yb is treated as fully 'conservative', seem to provide a useful way of recognizing elements affected by inferred subduction input, from more conservative elements. Based on such graphical comparisons, the following order of increasing 'subduction signature' is suggested: HREE, Ti (no discernible signature) < MREE, Zr, Nb < LREE, Y < Th < U, Pb, K, Sr, Ba, Sc, Cs. The corresponding levels of subduction input calculated by application of the Stolper & Newman 'H_2O-rich component' composition model range from zero to ~0·005 weight fractions. The overlapping trace element arrays between Tonga and the Kermadecs, in spite of inferred differences in sediment contribution, are thought to result from re-equilibration within the mantle wedge (Stolper & Newman, 1994).

Of particular note is the behaviour of Zr, Nb, and Y, each considered highly to very highly incompatible and insoluble elements (with Ti and Yb) in the spinel lherzolite oceanic arc wedge environment by Pearce & Parkinson

Table 3: Distribution coefficients used in trace element melting models

	Olivine	Clinopyroxene	Orthopyroxene	Spinel
Rb	0·0002	0·011	0·0006	0·0001
Ba	0·009	0·077	0·001	0·0001
Sr	0·0002	0·10	0·07	0·0001
Zr	0·0005	0·10	0·05	0·015
Y	0·015	0·70	0·15	0·005
Ni	13·2	2·0	4·5	8·8
Nb	0·001	0·05	0·01	0·015
La	0·0021	0·210	0·0046	0·0003
Ce	0·0022	0·297	0·0069	0·0004
Nd	0·0022	0·480	0·0104	0·0004
Sm	0·0023	0·565	0·0203	0·0004
Eu	0·0023	0·649	0·0258	0·0005
Gd	0·0024	0·758	0·0651	0·0005
Yb	0·015	0·750	0·200	0·0006
Lu	0·022	0·733	0·235	0·0008
Cr	1·5	10·0	7·0	150
Sc	0·2	2·0	1·0	0·2
V	0·03	0·8	0·3	10·0
Ti	0·01	0·4	0·25	0·15

K, Pb, Ta, Th, U, Cs, Zn, Cu and Sc also run using the bulk partition coefficient values of Stolper & Newman (1994). Initial mineral assemblage of fertile MORB mantle (FMM) is assumed to be: Olivine 0·585; Clinopyroxene 0·125; Orthopyroxene 0·270; Spinel 0·020 (weight fractions). Composition of FMM after Pearce & Parkinson (1993).

(1993). Although these elements apparently behave less conservatively within the Tonga–Kermadec–Lau system, this is thought to result from the influence of the Samoan plume input into the northernmost Tongan melt sources, as discussed above, with Nb most affected because of its high concentration in OIB relative to N-MORB melt sources.

Isotope–trace element results

To investigate possible balances between differing subduction inputs (e.g. changing role of sediment input north and south of the LR-SMC), changing rates of subduction (subduction rates increase northwards along the arc), and differing degrees of mantle source depletion, Sr, Pb and Nd isotopic data have also been modelled (Fig. 13).

Three endmembers were chosen (Table 4). The first is the mantle wedge, based on the average isotopic compositions of both ODP Sites 834 ('Pacific' MORB) and 836 ('Indian' MORB; Hergt & Hawkesworth, 1994). The second is altered oceanic crust, with Sr and Nd isotopic compositions from Staudigel *et al.* (1995) and Pb isotope composition based on sediment data from Unit 1 from DSDP Site 204 (Table 1), there being few other regionally applicable data. The third endmember is the LR-SMC, with Pb and Sr isotopic composition from Cheng *et al.* (1987), and Sr isotopic composition from Units 2 and 3, DSDP Site 204 (this paper). The modelling assumes, therefore, that the 'H$_2$O-rich component' has two possible isotopic endmember compositions, one corresponding to altered oceanic crust, and the second to the LR-SMC. Abundances of Sr, Nd, and Pb follow the Stolper & Newman (1994) estimates for the 'H$_2$O-rich component' (as used above); to some extent, this takes into account the decoupling of the various elements. Weight fractions of 0·001, 0·005, and 0·01 of the 'H$_2$O-rich component' are again added to the model depleted mantle wedge sources (FMM, RMM5 to RMM15), and second stage melt compositions are calculated. Some representative results are shown in Fig. 13, in which calculated ^{87}Sr/^{86}Sr, ^{143}Nd/^{144}Nd and ^{207}Pb/^{204}Pb are plotted against Pb, Zr, Nd, and Ti (variably 'conservative' elements). These calculated trends are compared with the normalized arc and back-arc element abundances, and the averaged isotopic compositions for each arc and back-arc volcanic centre. Each plot shows the effects of progressive subduction input on the second stage melts derived from each variably depleted mantle source composition (FMM, RMM5, etc.), and the
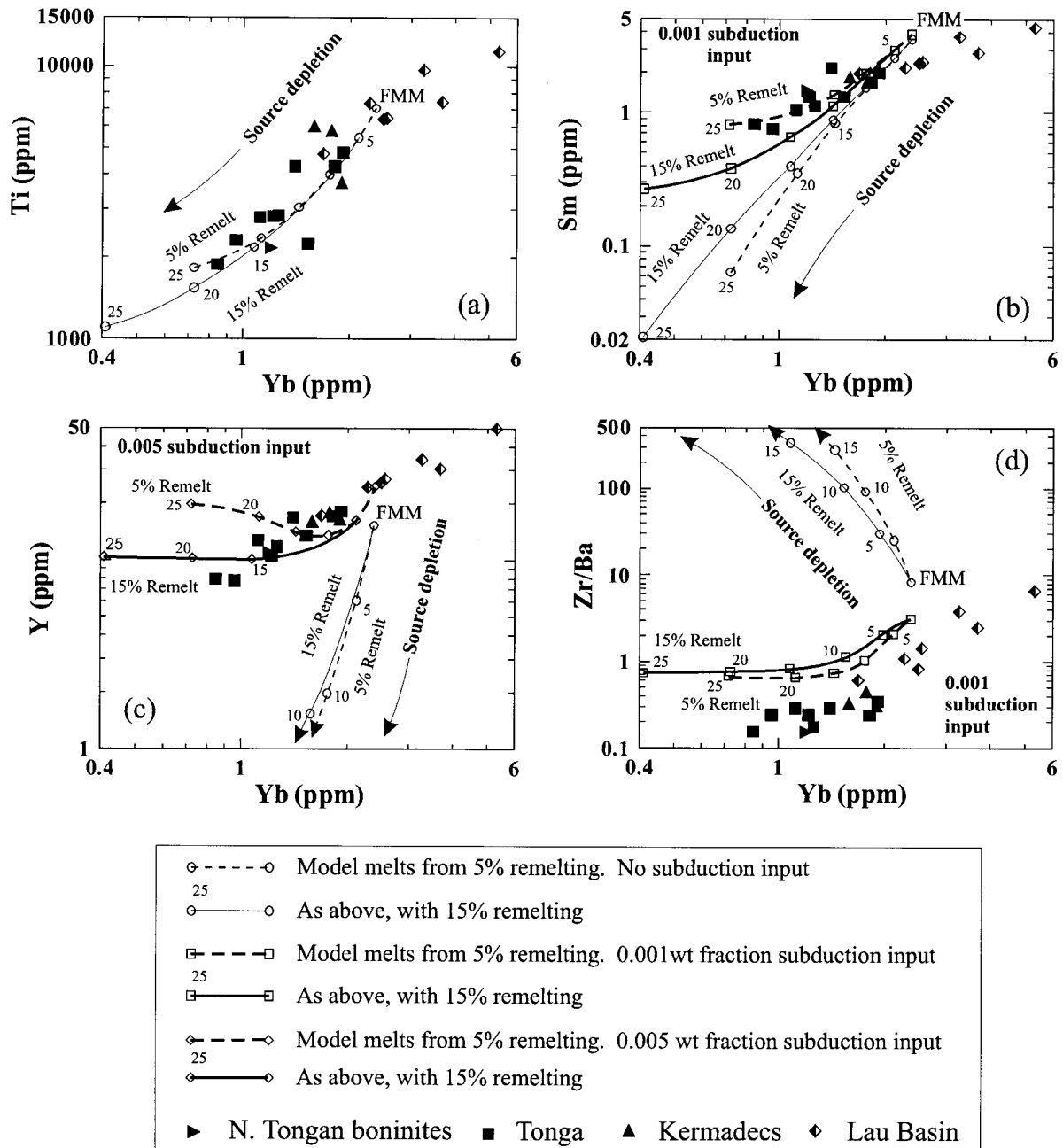
Fig. 12. Calculated melt composition for 5 and 15% remelting of previously depleted model mantle wedge compositions (corresponding to FMM to RMM25 compositions, as defined in the text; numbers along curves are percentage of prior melt extraction) for: (a) Yb, Ti (both apparently unaffected by subduction); (b) Sm (minor subduction effect); (c) Y (moderate subduction effect); (d) Zr/Ba ('subduction index'). These curves are compared, in each plot, with the normalized (MgO = 6%) data, from individual volcanic centres or sites, for Tonga, Kermadecs, and Lau Basin. In (b) and (d), calculated effects of addition of 0·001, and in (c) 0·005, wt fractions of 'H₂O-rich component' to the variously depleted model mantle wedge sources, followed by 5 and 15% remelting, are shown (curves with hollow diamonds and squares).
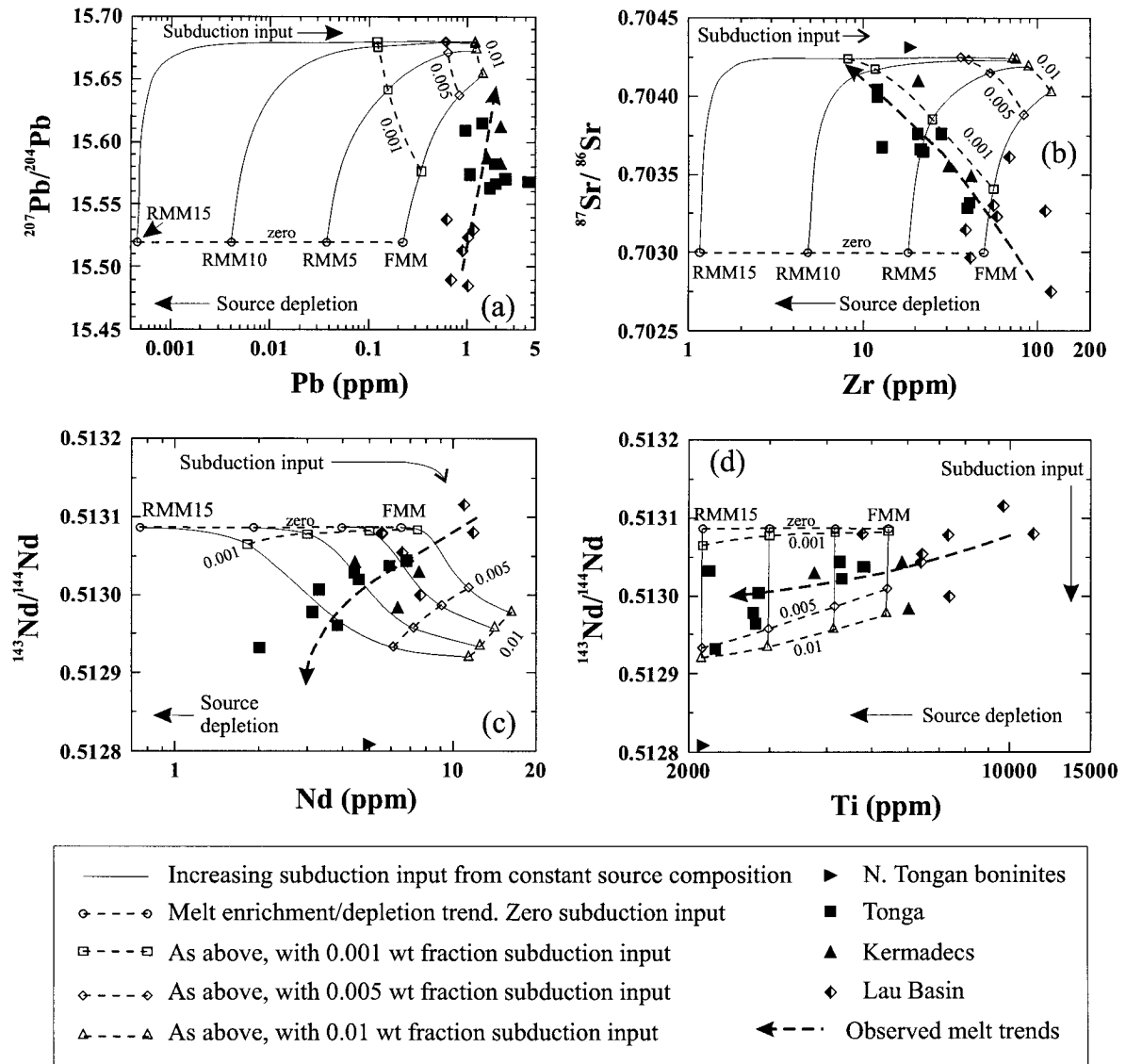
Fig. 13. Calculated isotopic and trace element melt compositions for 15% remelting of previously depleted model mantle wedge compositions (FMM to RMM15), assuming zero, 0·001, 0·005, and 0·01 weight fraction of 'H₂O-rich component' added to these sources. The continuous lines show increasing weight fractions of 'H₂O-rich component' to the source, up to 0·01 from each given starting model mantle composition (FMM to RMM15). The dotted curves mark combined source depletion plus constant subduction input to source trends (for zero, 0·001, 0·005, and 0·01 weight fraction inputs of 'H₂O-rich component'). The calculated curves are compared with normalized (MgO = 6%) data for individual volcanic centres or sites, for Tonga, Kermadecs, and Lau Basin. In (a) and (b), the altered oceanic crust isotopic endmember is used, whereas in (c) and (d), the LR-SMC isotopic endmember is used.

dashed lines mark the combined trends of variable source depletion with superimposed constant subduction input (i.e. 'equi-H₂O-rich component' lines).

Whereas the Sr and Pb isotope plots (Fig. 13a and b) utilize the altered oceanic crust, the Nd isotopic endmember requires a relatively less radiogenic composition than the altered oceanic crust data of Staudigel *et al.* (1995). In Fig. 13c, the LR-SMC endmember composition is therefore used, although even this composition does not

possess su ciently unradiogenic Nd to explain the northern Tongan boninite compositions. This further supports a Samoan plume component in these boninites, as previously discussed.

Three general patterns of element behaviour are illustrated by Fig. 13:

(1) Elements for which the subduction input has e ectively swamped any original source variations (e.g. prior depletion e ects), as shown by Pb (Fig. 13a); other elements

Table 4: Endmember isotopic compositions used in subduction input models

	Mantle wedge*	LR-SMC	Altered oceanic crust
$^{87}Sr/^{86}Sr$	0·702992	0·705195†	0·70425‡
$^{143}Nd/^{144}Nd$	0·513085	0·512911	0·513057‡
$^{206}Pb/^{204}Pb$	18·549	19·285	18·825§
$^{207}Pb/^{204}Pb$	15·519	15·614	15·680§
$^{208}Pb/^{204}Pb$	38·153	39·027	38·845§

*Average of ODP Sites 834 and 836.
†Sediments from Units 2 and 3, DSDP Site 204.
‡After Staudigel *et al.* (1995).
§Unit 1, DSDP Site 204; element abundances used for the assumed subduction component are taken from the 'H₂O-rich component' of Stolper & Newman (1994).

with similar behaviour are Rb, Ba, Sr, K, Cs, Th, U, and Sc, which agrees well with the experimental partitioning data of Keppler (1996).

(2) Elements showing subduction effects and following 'iso-H₂O component' trends (typically at ~0·001–0·005 weight fractions), but where abundances still reflect variations in source depletion composition, as shown by $^{87}Sr/^{86}Sr$–Zr and $^{144}Nd/^{143}Nd$–Nd (Fig. 13b and c). Other elements showing this style of behaviour are La, Ce, Y, and Nb (this last element complicated by the Samoan input into northern Tonga).

(3) Elements least affected by subduction input (Fig. 13d), illustrated by MREE to HREE (Sm to Lu), and Ti, whose abundances are therefore strongly controlled by mantle wedge source compositions.

In summary, the isotope–trace element modelling (Fig. 13) supports the trace element modelling (Fig. 12), and is consistent with subducted altered oceanic crust as a source of Sr and Pb in Tonga lavas. $^{143}Nd/^{144}Nd$ is more problematic, and requires a less radiogenic Nd composition than may be typical of altered ocean floor basalts alone. In view of the 'semi-conservative' behaviour of Nd, this may reflect an unradiogenic component in the mantle wedge, derived either from Samoa OIB mantle or even from sedimentary material introduced during previous subduction events. The combined trace element and trace element–isotope modelling suggests that the coupled processes of mantle wedge depletion with input of subduction fluid (at <0·001–0·005 weight fraction abundances) can explain the geochemistry of these arc–back-arc lavas. The correlations in Tonga–Lau between isotopic compositions and geochemical source depletion indicators (e.g. Yb, Ti, Zr), together with the observed isotopic variation along the Tongan arc, are inferred to result from a relatively constant subduction flux into a mantle wedge which is progressively more depleted to the east (Lau Basin) and north (Tonga).

This is considered a significant conclusion to result from the new data presented in this work.

BACK-ARC AND ARC EVOLUTION—TEMPORAL VARIATIONS WITHIN THE TONGA–LAU SYSTEM

The scenario of mantle wedge depletion and subduction zone enrichment has possible temporal implications: (1) in some way, the degree of mantle source depletion will depend on, and thus correlate with, the extent of back-arc volcanism; (2) the inferred wedge depletion may become cumulative where a succession of arcs and back-arc systems have sequentially developed in the same region, as is the case in the Lau–Colville–Tonga–Kermadec systems (Yan & Kroenke, 1993). Superimposed subduction zone enrichment to the melt sources will, however, presumably cause differential blurring of these effects.

It is therefore relevant to compare the geochemistry of the modern arc with the older arc volcanic phases, namely the Tongan proto-arc construct (ODP Site 839), the LVG and KVG of the Lau Ridge, and the Mid to Early Tertiary volcanics of the Tongan Ridge basement. The modern Tongan lavas show evidence for more intense source depletion than the older arc lavas of the region (Fig. 3). The combined isotope–element ratio plots (Figs 7 and 8) indicate that the older arc lavas have lower relative subduction input than the modern arc lavas, consistent with a less depleted mantle wedge. Note is further made of the intermediate trace element and isotopic compositional arrays of the ODP Site 839 lavas, between Lau Basin and modern Tonga and Kermadec lavas.

The overall implication is that there has been a tendency for the sub-arc and back-arc mantle wedge to have become

progressively more depleted since at least the Late Tertiary, now seen at its most extreme in northernmost Tonga. This implies a long 'residence time' for mantle material within the wedge, and again emphasizes the coupling between arc and back-arc magmatism. Clearly, however, fresh asthenospheric influxes have punctuated the mantle wedge evolution, as seen in upwelling of non-subduction-modified 'Indian' MORB mantle in the Lau Basin, and southward flow of mantle containing a Samoa plume component beneath the northern end of the Tonga arc. A model depicting the possible temporal evolution of the Lau–Tonga system has been presented schematically by Ewart *et al.* (1994*a*). This assumes that the arc–back-arc developed as a coupled system, with imbrication of the subducting slab initiating Lau Basin opening, also possibly a mechanism allowing influx of 'Indian' MORB mantle southwards into the sub-Lau Basin mantle. This model further implies relatively long-lived recycling within the mantle wedge.

CONCLUSIONS

(1) The new data confirm (compare Hawkins *et al.*, 1994) the existence of gradients in trace element and isotope chemistry between the Tonga–Lau arc and back-arc lavas. These range from arc-like (northern Tonga) to N-MORB-like (western and central Lau Basin). The new data also emphasize the distinctive OIB-like geochemistry of the Samoan, LR-SMC, and MVG lavas. The arc and back-arc data define apparent mixing trends in element ratio plots, but although sediments lie near one end of these arrays, the data do not support mixing of the bulk sediment with the arc melts or melt sources. Nevertheless, the trace element–isotope arrays do seem to display complex mixing curves, between a 'subduction' component (broadly defined by the sediment data) and 'older' and 'new' Lau Basin N-MORB mantle sources.

(2) Comparison of the Pb isotope compositions of the arc lavas with 'Indian' and 'Pacific' MORB and Pacific sediment suggests that the Kermadec and Tongan lavas reflect mixtures of Pb from Pacific sediment and altered Pacific ocean crust, the Kermadec lavas having a larger sedimentary component. Northern Tonga lavas contain Pb derived from the subducting LR-SMC.

(3) Along-arc variations of Pb, Sr and Pb isotopic compositions, and many trace element parameters (e.g. Zr/Ba, Th/Pb, Ti/Zr, Zr/Sm, Sc/Y ratios, and Ti, Yb, and Y abundances), are observed. These show systematic gradients, except for sharp changes of Pb isotopes at the extreme northern end of Tonga. These reflect differences in the amounts, and compositions of material being subducted along the arc (e.g. LR-SMC in northern Tonga), and variations in the degree of mantle wedge depletion.

(4) Trace element data (best illustrated in MgO = 6% normalized plots for individual volcanic centres) support mantle wedge source depletion in the Lau Basin and sub-arc mantles, attributed to melt extraction processes within the back-arc. The degree of depletion increases northwards along both the Tongan and Kermadec arcs, correlating with the degree of back-arc extension. The sub-arc melt sources are more depleted than the back-arc. The evidence from the older Tongan 'proto-arc' (Site 839), the LVB and KVG (Lau Ridge), and the older Tertiary arc volcanics of the Tongan Ridge suggest that the depletion effect is cumulative, implying a long 'residence time' of mantle within the wedge.

(5) The isotopic data favour an 'LR-SMC component' in the melt source of the two northern Tongan volcanoes of Tafahi and Niuatoputapu, whereas relatively high Nb abundances suggest minor Samoan plume input. The boninitic lavas at the extreme northern end of the Tongan arc show evidence from isotopic and HFSE compositions for a significant Samoan plume input to their asthenospheric melt sources. These different elements were introduced into the arc lavas from the Samoan and Louisville plumes by fundamentally different mechanisms.

(6) The Tongan and Kermadec lavas show differences in certain trace element and isotopic characteristics. Th/U is a key ratio showing a consistent difference, which is reflected in differences in ^{230}Th–^{238}U systematics (Regelous *et al.*, 1997). The Kermadec data arrays extend closest to, and overlap the sediment data (excepting the DSDP Site 204 data for the LR-SMC derived sediments) relative to Tonga. This suggests that a subducted sediment component is important in the Kermadec arc melt sources, whereas in Tonga, altered oceanic crust is the dominant source of most 'non-conservative' elements, most clearly shown by the LR-SMC Pb isotope signature in northern Tonga lavas. This difference between the Tonga and Kermadec arcs can be related to differences in the amount of sediment being subducted beneath the two arc segments.

(7) F and CO_2 exhibit higher abundances in the arc compared with back-arc lavas, with the 'proto-Tonga Arc' (ODP Site 839) intermediate. These differences are present in spite of the expected degassing effects in the subaerially erupted arc lavas, suggesting their primary melt abundances to have been even more elevated. Polybaric degassing and fractional crystallization are inferred to have affected the volatile abundances within the back-arc lavas.

(8) Niua fo'ou, the only active subaerial volcano within the Lau Basin, is distinct in its trace element and isotopic compositions from any of the other Lau Basin, arc, Samoan, or LR-SMC lavas. It is also relatively enriched in F and CO_2, similar to the arc lavas. It is suggested that it represents a separate 'mini-plume' from deeper within the Lau Basin, possibly involving mixing of the 'new' (Indian) Lau Basin MORB-source with a restricted isotopic subset

of the Samoan plume arrays (plausibly the post-erosional melts or their source).

(9) Trace element and isotopic modelling suggests that MREE to HREE and Ti are least affected by subduction input, with LREE, Zr, Nb and Y showing minor modification, whereas U, Pb, K, Sr, Ba, and Sc have strong subduction input effects, effectively swamping primary source compositional differences. Using the 'H₂O-rich component' model of Stolper & Newman (1994), levels of 0·001–0·005 weight fractions are suggested to have been added to the arc sources. The calculated isotope and trace element curves duplicate observed data trends from back-arc to arc, by modelling the simultaneous effects of source depletion and subduction input. Modelling suggests that the trace element variations within the Tonga–Lau Basin data, and the variations observed along the Tonga arc, can be explained by variations in the degree of source depletion, at relatively constant subduction component fluxes.

ACKNOWLEDGEMENTS

REFERENCES

Bodkin, J. B. (1977). Determination of fluorine in silicates by use of an ion-selective electrode following fusion with lithium metaborate. *The Analyst* **102**(1215), 409–413.

Boespflug, B., Dosso, L., Bougault, H. & Joron, J.-L. (1990). Trace element and isotopic (Sr, Nd) geochemistry of volcanic rocks from the Lau Basin. In: von Stackelberg, U. & von Rad, U. (eds) *Geological Evolution and Hydrothermal Activity in the Lau and North Fiji Basins, Southwest Pacific Ocean (Results of SONNE Cruise SO-35). Geologische Jahrbuch* **92**, 503–516.

Burns, R. E., Andrews, J. E. *et al.* (1973). Site 204. In: *Initial Reports of the Deep Sea Drilling Project, 21*. Washington: US Government Printing Office, pp. 33–56.

Cheng, Q., Park, K.-H., Macdougall, J. D., Zindler, A., Lugmair, G. W., Staudigel, H., Hawkins, J. & Lonsdale, P. (1987). Isotopic evidence for a hotspot origin of the Louisville seamount chain. In: Keating, B., Fryer, P., Batiza, R. & Boehlert, G.W. (eds) *Seamounts, Islands, and Atolls. Geophysical Monograph, American Geophysical Union* **43**, 283–296.

Cole, J. W., Graham, I. J. & Gibson, I. L. (1990). Magmatic evolution of Late Cenozoic volcanic rocks of the Lau Ridge, Fiji. *Contributions to Mineralogy and Petrology* **104**, 540–554.

Danyushevsky, L. V., Sobolev, A. V. & Falloon, T. J. (1995). North Tongan high-Ca boninite petrogenesis: the role of Samoan plume and subduction zone–transform fault transition. *Journal of Geodynamics* **20**, 219–241.

Davey, F. J., Hampton, M., Childs, J., Fisher, M. A., Lewis, K. B. & Pettinga, J. R. (1986). Structure of a growing accretionary prism, Hikurangi margin, New Zealand. *Geology* **14**, 663–666.

Davies, J. H. & Bickle, M. J. (1991). A physical model for the volume and composition of melt produced by hydrous fluxing above subduction zones. *Philosophical Transactions of the Royal Society of London, Series A* **335**, 355–364.

Davies, J. H. & Stevenson, D. J. (1992). Physical model of source region of subduction zone volcanics. *Journal of Geophysical Research* **97**, 2037–2070.

DeMets, C., Gordon, R. G., Argus, D. F. & Stein, S. (1990). Current plate motions. *Geophysical Journal International* **101**, 425–478.

Dixon, J. E. & Stolper, E. M. (1995). An experimental study of water and carbon dioxide solubilities in mid-ocean ridge basaltic liquids. Part II: Applications to degassing. *Journal of Petrology* **36**, 1633–1646.

Ewart, A. & Hawkesworth, C. J. (1987). The Pleistocene–Recent Tongan–Kermadec arc lavas: interpretation of new isotope and rare earth data in terms of a depleted mantle source model. *Journal of Petrology* **28**, 295–330.

Ewart, A., Bryan, W. B. & Gill, J. (1973). Mineralogy and geochemistry of the younger volcanic islands of Tonga, southwest Pacific. *Journal of Petrology* **14**, 429–465.

Ewart, A., Brothers, R. N. & Mateen, A. (1977). An outline of the geology and geochemistry, and the possible petrogenetic evolution of the volcanic rocks of the Tonga–Kermadec–New Zealand island arc. *Journal of Volcanology and Geothermal Research* **2**, 205–250.

Ewart, A., Bryan, W. B., Chappell, B. W. & Rudnick, R. L. (1994a). Regional geochemistry of the Lau–Tonga arc and back-arc systems. In: Hawkins, J., Parson, L., Allan, J. *et al.* (eds) *Proceedings of the Ocean Drilling Program, Scientific Results 135*. College Station, TX: Ocean Drilling Program, pp. 385–425.

Ewart, A., Hergt, J. M. & Hawkins, J. W. (1994b). Major element, trace element, and isotope (Pb, Sr and Nd) geochemistry of Site 839 basalts and basaltic andesites: implications for arc volcanism. In: Hawkins, J., Parson, L., Allan, J. *et al.* (eds) *Proceedings of the Ocean Drilling Program, Scientific Results 135*. College Station, TX: Ocean Drilling Program, pp. 519–531.

Falloon, T. J. & Crawford, A. J. (1991). The petrogenesis of high-calcium boninite lavas dredged from the northern Tongan ridge. *Earth and Planetary Science Letters* **102**, 375–394.

Falloon, T. J., Green, D. H. & Crawford, A. J. (1987). Dredged igneous rocks from the northern termination of the Tofua magmatic arc, Tonga and adjacent Lau Basin. *Australian Journal of Earth Sciences* **34**, 487–506.

Falloon, T. J., Green, D. H. & McCulloch, M. T. (1989). Petrogenesis of high-Mg and associated lavas from the north Tonga trench. In: Crawford, A. J. (ed.) *Boninites and Related Rocks*. London: Unwin Hyman, pp. 357–395.

Farley, K. A., Natland, J. H. & Craig, H. (1992). Binary mixing of enriched and undegassed (primitive?) mantle components (He, Sr, Nd, Pb) in Samoan lavas. *Earth and Planetary Science Letters* **111**, 183–199.

Ferguson, E. M. & Klein, E. M. (1993). Fresh basalts from the Pacific–Antarctic Ridge extend the Pacific geochemical province. *Nature* **366**, 330–333.

Gamble, J. A. & Wright, I. C. (1995). The Southern Havre Trough. Geological structure and magma petrogenesis of an active back-arc

rift complex. In: Taylor, B. (ed.) *Back-arc Basins: Tectonics and Magmatism.* New York: Plenum, pp. 29–62.

Gamble, J. A., Wright, I. C. & Baker, J. A. (1993). Seafloor geology and petrology in the oceanic to continental transition zone of the Kermadec–Havre–Taupo Volcanic Zone arc system, New Zealand. *New Zealand Journal of Geology and Geophysics* **36,** 417–435.

Gamble, J. A., Wright, I. C., Woodhead, J. D. & McCulloch, M. T. (1995). Arc and back-arc geochemistry in the southern Kermadec arc–Ngatoro Basin and o shore Taupo Volcanic Zone, SW Pacific. In: Smellie J. L. (ed.) *Volcanism Associated with Extension at Consuming Plate Margins. Geological Society, London, Special Publication* **81,** 193–212.

Gamble, J., Woodhead, J., Wright, I. & Smith, I. (1996). Basalt and sediment geochemistry and magma petrogenesis in a transect from oceanic island arc to rifted continental margin arc: the Kermadec–Hikurangi margin, SW Pacific. *Journal of Petrology* **37,** 1523–1546.

Giardini, D. & Woodhouse, J. H. (1986). Horizontal shear flow in the mantle beneath the Tonga arc. *Nature* **319,** 551–555.

Harris, D. M. & Anderson, A. T. (1984). Volatiles H_2O, CO_2, and Cl in a subduction related basalt. *Contributions to Mineralogy and Petrology* **87,** 120–128.

Hawkins, J. W. & Lonsdale, P. F. (1987). Petrologic evolution of the Louisville seamount chain. In: Keating, B., Fryer, P., Batiza, R. & Boehlert, G. W. (eds) *Seamounts, Islands and Atolls. Geophysical Monograph, American Geophysical Union* **43,** 235–254.

Hawkins, J., Parson, L., Allan, J. *et al.* (eds) (1994). *Proceedings of the Ocean Drilling Program, Scientific Results 135.* College Station, TX: Ocean Drilling Program.

Hergt, J. M. & Hawkesworth, C. J. (1994). Pb-, Sr-, and Nd-isotopic evolution of the Lau Basin: implications for mantle dynamics during back-arc opening. In: Hawkins, J., Parson, L., Allen, J. *et al.* (eds) *Proceedings of the Ocean Drilling Program, Scientific Results 135.* College Station, TX: Ocean Drilling Program, pp. 505–517.

Hickey-Vargas, R., Hergt, J. M. & Spadea, P. (1995). The Indian Ocean-type isotopic signature in western Pacific marginal basins: origin and significance. In: *Active Margins and Marginal Basins of the Western Pacific, Geophysical Monograph, American Geophysical Union* **88,** 175–197.

Jarrard, R. D. (1986). Relations among subduction parameters. *Reviews of Geophysics* **24,** 217–284.

Jenner, G. A., Cawood, P. A., Rautenschlein, M. & White, W. M. (1987). Composition of back-arc basin volcanics, Valu Fa Ridge, Lau Basin: evidence for a slab-derived component in their mantle source. *Journal of Volcanology and Geothermal Research* **32,** 209–222.

Karig, D. E. (1970). Ridges and basins of the Tonga–Kermadec island arc system. *Journal of Geophysical Research* **75,** 239–254.

Kennett, J. P., Houtz, R. E. *et al.* (1974). Site 275. In: *Initial Reports of the Deep Sea Drilling Project, 29.* Washington, DC: US Government Printing O ce, pp. 19–35.

Keppler, H. (1996). Constraints from partitioning experiments on the composition of subduction-zone fluids. *Nature* **380,** 237–240.

Loock, G., McDonough, W. F., Goldstein, S. L. & Hofmann, A. W. (1990). Isotopic compositions of volcanic glasses from the Lau Basin. *Marine Mining* **9,** 235–245.

Macpherson, C. & Mattey, D. (1994). Carbon isotope variations of CO_2 in central Lau Basin basalts and ferrobasalts. *Earth and Planetary Science Letters* **121,** 263–276.

Manhes, G., Minster, J. F. & Allègre, C. J. (1978). Comparative uranium–thorium–lead and rubidium–strontium study of the Saint Severin amphoterite: consequences for early solar system chronology. *Earth and Planetary Science Letters* **39,** 14–24.

Menard, H. W., Natland, J., Jordan, T. H., Orcutt, J. A. *et al.* (1987). Site 596: hydraulic piston coring in an area of low surface productivity in the southwest Pacific. In: *Initial Reports of the Deep Sea Drilling Project,* 91. Washington, DC: US Government Printing O ce, pp. 245–267.

Muhe, R., Peucker-Ehrenbrink, B., Devey, C. W. & Garbe-Schonberg, D. (1997). On the redistribution of Pb in the oceanic crust during hydrothermal alteration. *Chemical Geology* **137,** 67–77.

Newsom, H. E., White, W. M., Jochum, K. P. & Hofmann, A. W. (1986). Siderophile and chalcophile element abundances in oceanic basalts, Pb isotope evolution and growth of Earth's core. *Earth and Planetary Science Letters* **80,** 299–313.

Niu, Y. & Hékinian, R. (1997). Basaltic liquids and harzburgitic residues in the Garrett Transform: a case study at fast-spreading ridges. *Earth and Planetary Science Letters* **146,** 243–258.

Norrish, K. & Hutton, J. T. (1969). An accurate X-ray spectrographic method for the analysis of a wide range of geological samples. *Geochimica et Cosmochimica Acta* **33,** 431–453.

Palacz, Z. A. & Saunders, A. D. (1986). Coupled trace element and isotope enrichment in the Cook–Austral–Samoa islands, southwest Pacific. *Earth and Planetary Science Letters* **79,** 270–280.

Parson, L., Hawkins, J., Allan, J. *et al.* (1992). *Proceedings of the Ocean Drilling Program, Initial Reports, Part 1, 135.* College Station, TX: Ocean Drilling Program.

Pearce, J. A. & Parkinson, I. J. (1993). Trace element models for mantle melting: application to volcanic arc petrogenesis. In: Prichard, H. M., Alabaster, T., Harris, N. B. W. & Neary, C. R. (eds) *Magmatic Processes and Plate Tectonics. Geological Society, London, Special Publication* **76,** 373–403.

Pearce, J. A. & Peate, D. W. (1995). Tectonic implications of the composition of volcanic arc magmas. *Annual Review of Earth and Planetary Sciences* **23,** 251–285.

Pearce, J. A., Baker, P. E., Harvey, P. K. & Lu , I. W. (1995). Geochemical evidence for subduction fluxes, mantle melting and fractional crystallization beneath the South Sandwich Island Arc. *Journal of Petrology* **36,** 1073–1109.

Reay, A., Rooke, J. M., Wallace, R. C. & Whelan, P. (1974). Lavas from Niuafo'ou Island, Tonga, resemble ocean-floor basalts. *Geology* **2,** 605–606.

Regelous, M., Collerson, K. D., Ewart, A. & Wendt, J. I. (1996). Two mantle plumes contribute to island-arc magmatism in northern Tonga. *EOS Transactions, American Geophysical Union* **77**(46), 842 (abstract).

Regelous, M., Collerson, K. D., Ewart, A. & Wendt, J. I. (1997). Trace element transport rates in subduction zones: evidence from Th, Sr and Pb isotope data for Tonga–Kermadec lavas. *Earth and Planetary Science Letters* **150,** 291–302.

Sager, W. W., MacLeod, C. J. & Abrahamsen, N. (1994). Paleomagnetic constraints on Tonga arc rotation from sediments drilled at Sites 840 and 841. In: Hawkins, J., Parson, L., Allan, J. *et al.* (eds) *Proceedings of the Ocean Drilling Program, Scientific Results 135.* College Station, TX: Ocean Drilling Program, pp. 763–783.

Shaw, D. M. (1970). Trace element fractionation during anatexis. *Geochimica et Cosmochimica Acta* **34,** 237–243.

Staudigel, H., Davies, G. R., Hart, S. R., Marchant, K. M. & Smith, B. M. (1995). Large scale isotopic Sr, Nd and O isotopic anatomy of altered oceanic crust: DSDP/ODP sites 417/418. *Earth and Planetary Science Letters* **130,** 169–185.

Stolper, E. & Newman, S. (1994). The role of water in the petrogenesis of Mariana Trough magmas. *Earth and Planetary Science Letters* **121,** 293–325.

Sunkel, G. (1990). Origin of petrological and geochemical variations of Lau Basin lavas (SW Pacific). *Marine Mining* **9,** 205–234.

Tatsumi, Y., Hamilton, D. L. & Nesbitt, R. W. (1986). Chemical characteristics of fluid phase released from a subducted lithosphere and origin of arc magmas: evidence from high-pressure experiments and natural rocks. *Journal of Volcanology and Geothermal Research* **29,** 293–309.

Turek, A., Riddle, C., Cozens, B. J. & Tetley, N. W. (1976). Determination of chemical water in rock analysis by Karl Fischer titration. *Chemical Geology* **17,** 261–267.

Turek, A., Riddle, C. & Talerico, F. (1978). Determination of carbon dioxide in rock analysis by non-aqueous titration. *Chemical Geology* **21,** 351–357.

Turner, S., Hawkesworth, C. J., Bartlett, J., Rogers, N. W., Smith, I. & Worthington, T. (1996). U–Th disequilibria, along the Tonga–Kermadec island arc. *1996 Goldschmidt Conference Abstracts* **630**.

Turner, S., Hawkesworth, C. J., Rogers, N. W., Bartlett, J., Smith, I. & Worthington, T. (1997). U-series disequilibria, magma petrogenesis and flux rates along the depleted Tonga–Kermadec island arc. *Geological Society of Australia Abstracts* **45,** 95–98.

Vallier, T. L., Stevenson, A. J. & Scholl, D. W. (1985). Petrology of igneous rocks from 'Ata Island, Kingdom of Tonga. In: Scholl, D. W. & Vallier, T. L. (eds) *Geology and Offshore Resources of Pacific Island Arcs—Tonga Region. Circum-Pacific Council for Energy and Mineral Resources, Earth Science Series* **2,** 301–316.

Vallier, T. L., Jenner, G. A., Frey, F. A., Gill, J. B., Davis, A. S., Volpe, A. M., Hawkins, J. W., Morris, J. D., Cawood, P. A., Morton, J. L., Scholl, D. W., Rautenschlein, M., White, W. M., Williams, R. W., Stevenson, A. J. & White, L. D. (1991). Subalkaline andesite from Valu Fa Ridge, a back-arc spreading center in southern Lau Basin: petrogenesis, comparative chemistry, and tectonic implications. *Chemical Geology* **91,** 227–256.

Volpe, A. M., Macdougall, J. D. & Hawkins, J. W. (1988). Lau Basin basalts (LBB): trace element and Sr–Nd isotopic evidence for heterogeneity in back-arc basin mantle. *Earth and Planetary Science Letters* **90,** 174–186.

von Stackelberg, U. & Shipboard Scientific Party (1985). Hydrothermal sulphide deposits in back-arc spreading centres in the southwest Pacific. *Bundesanstalt für Geowissenschaften und Rohstoffe Circular* **2,** 3–14.

Wendt, J. I., Regelous, M., Collerson, K. D. & Ewart, A. (1997). Evidence for the role of two mantle plumes in island arc lavas from northern Tonga. *Geology* **25,** 611–614.

Woodhead, J., Eggins, S. & Gamble, J. (1993). High field strength and transition element systematics in island arc and back-arc basin basalts: evidence for multi-phase melt extraction and a depleted mantle wedge. *Earth and Planetary Science Letters* **114,** 491–504.

Wright, E. & White, W. M. (1987). The origin of Samoa: new evidence from Sr, Nd, and Pb isotopes. *Earth and Planetary Science Letters* **81,** 151–162.

Yan, C.-Y. & Kroenke, L. W. (1993). A plate tectonic reconstruction of the southwest Pacific, 0–100 Ma. In: *Proceedings of the Ocean Drilling Program, Scientific Results 130*. College Station, TX: Ocean Drilling Program, pp. 697–709.

APPENDIX

Table A1: Selected new ICP-MS trace element analyses and Ti, F, CO_2 and H_2O^+ of Tonga–Kermadec lavas (all values in ppm except H_2O^+, in wt %)

	TONGA						Niuatoputapu				
Island:	Tafahi										
Sample:	T068	T069	T072	T073	T113	T116	NT051	NT052A	NT 053	NT054	NT64-T2
Rock type:	BA	B	B	BA	BA	BA	BA	BA	A	BA	A
Li	—	—	—	—	3·34	2·30	—	—	—	—	5·60
Be	0·22	0·18	0·20	0·21	0·19	0·18	0·30	0·31	0·597	0·30	0·33
Sc	46·35	46·8	46·8	43·0	49·9	43·9	48·2	51·8	42·4	49·5	46·2
V	271	282	273	299	284	298	281	394	285	274	352
Cr	—	—	—	—	80·6	52·0	299	42·9	0·051	539	1·38
Co	71·3	61·8	76·0	75·8	49·2	47·0	67·4	62·1	56·2	61·9	58·4
Ni	24·25	23·6	24·7	17·7	31·8	28·1	35·3	14·7	3·03	33·9	4·87
Cu	—	—	—	—	136	77·1	—	—	—	—	244
Zn	—	—	—	—	75·5	66·3	—	—	—	—	96·3
Ga	11·4	12·3	11·8	12·5	14·2	15·4	11·5	13·0	12·7	11·1	14·8
Rb	2·40	0·70	2·51	2·34	3·01	2·95	5·33	5·18	10·7	4·98	8·74
Sr	127	128	133	133	155	156	171	189	210	159	223
Y	8·21	8·23	8·31	9·74	8·13	7·88	7·27	11·5	15·0	6·41	10·9
Zr	11·9	10·8	11·0	13·1	12·7	11·7	11·5	13·7	25·7	11·0	24·1
Nb	0·70	0·45	0·59	0·50	0·79	0·46	1·15	0·90	2·30	1·10	1·53
Cs	0·077	0·019	0·086	0·079	0·077	0·078	0·144	0·114	0·203	0·129	0·18
Ba	57·2	32·4	44·1	41·1	48·8	45·2	73·9	78·8	162	76·4	139
La	1·19	0·828	1·07	0·923	1·17	0·885	1·87	2·18	4·60	1·69	2·72
Ce	2·69	1·99	2·37	2·28	3·15	2·62	3·76	4·09	8·01	3·40	6·78
Pr	0·392	0·324	0·364	0·378	0·365	0·286	0·543	0·697	1·29	0·499	0·916
Nd	1·95	1·71	1·83	2·05	2·23	2·09	2·54	3·34	6·02	2·28	4·06
Sm	0·704	0·658	0·687	0·787	0·802	0·769	0·784	1·05	1·77	0·688	1·21
Eu	0·279	0·728	0·279	0·327	0·253	0·251	0·290	0·394	0·615	0·272	0·459
Gd	1·035	0·986	1·03	1·20	1·03	0·985	1·07	1·50	2·34	0·964	1·62
Tb	0·204	0·186	0·189	0·226	0·182	0·178	0·179	0·245	0·381	0·156	0·261
Dy	1·27	1·28	1·26	1·49	1·23	1·22	1·13	1·56	2·38	1·00	1·79
Ho	0·292	0·297	0·291	0·344	0·279	0·274	0·256	0·366	0·530	0·229	0·404
Er	0·897	0·897	0·892	1·06	0·869	0·847	0·787	1·12	1·61	0·705	1·24
Tm	0·129	0·129	0·128	0·151	0·125	0·121	0·111	0·157	0·225	0·099	0·176
Yb	0·911	0·885	0·885	1·05	0·904	0·871	0·801	1·11	1·60	0·715	1·29
Lu	0·142	0·135	0·138	0·162	0·136	0·134	0·127	0·177	0·251	0·110	0·208
Hf	0·38	0·35	0·36	0·44	0·37	0·36	0·36	0·44	0·80	0·34	0·77
Ta	—	—	—	—	0·050	0·040	—	—	—	—	—
Pb	1·01	0·82	0·89	0·88	1·16	1·11	1·43	1·44	2·46	1·34	7·66
Th	0·199	0·109	0·164	0·108	0·201	0·131	0·360	0·287	0·776	0·35	0·508
U	0·095	0·085	0·081	0·065	0·127	0·099	0·105	0·107	0·223	0·099	0·235
Ti	1920	1920	1920	2460	2400	2160	1740	2280	3000	1620	3120
F	—	—	—	—	78	71	—	—	—	—	—
CO_2	—	—	—	—	260	250	—	—	—	—	—
H_2O^+	—	—	—	—	0·90	0·59	—	—	—	—	—

Table A1: continued

Island:	TONGA Fonualei						Late			Metis	Kao	
Sample:	F8	F20	F30	F31	F39	F41	L3	L20	L21	Metis Shoal (TR)	T101P	T102
Rock type:	D	D	A	A	D	D	DA	BA	BA	D	BA	BA
Li	8·71	—	5·59	5·95	—	7·97	4·94	—	4·97	9·90	5·70	4·9
Be	0·60	0·60	0·47	0·48	0·59	0·54	0·22	0·19	0·23	0·24	0·35	0·30
Sc	26·1	26·5	35·5	34·2	26·6	25·4	44·0	45·7	41·9	29·5	35·5	36·3
V	80·4	101	207	194	86·7	92·7	356	376	368	183	337	330
Cr	0·50	0·11	0·59	3·23	3·25	0·78	37·2	75·0	30·9	245	32·0	26·0
Co	17·0	14·1	28·4	27·1	13·6	18·2	41·1	36·2	42·3	30·4	33·7	35·9
Ni	3·22	1·15	5·12	5·01	2·27	4·28	27·4	25·3	27·0	56·0	22·2	21·4
Cu	26·6	28·0	53·2	45·2	26·0	38·9	169	150	172	91·5	131	122
Zn	119	115	114	108	113	102	84·5	86·0	90·0	61·0	83·0	87·0
Ga	15·5	14·3	16·9	16·4	14·2	16·0	16·0	14·1	16·8	11·4	16·2	15·1
Rb	15·6	14·0	10·6	11·6	15·4	13·5	7·23	5·73	6·88	13·2	7·09	6·30
Sr	289	290	297	302	288	295	219	211	228	135	304	235
Y	20·1	19·6	13·6	16·2	23·1	16·0	12·7	12·8	12·7	14·6	21·6	19·9
Zr	41·8	44·5	30·6	31·3	44·8	37·7	22·7	21·4	21·9	39·9	46·6	42·0
Nb	0·92	0·93	0·65	0·70	0·93	0·81	0·27	0·29	0·37	0·50	0·44	0·40
Cs	0·56	0·18	0·25	0·38	0·56	0·22	0·26	0·20	0·23	0·78	0·22	0·22
Ba	243	233	187	187	234	235	106	84·3	92·0	337	119	116
La	4·14	3·17	2·49	3·28	4·14	2·95	1·70	1·43	1·70	2·85	2·68	3·18
Ce	10·4	7·70	6·37	8·20	10·0	7·44	4·81	3·78	4·95	6·95	7·44	6·26
Pr	1·68	1·24	1·04	1·35	1·61	1·23	0·795	0·635	0·803	1·09	1·29	1·08
Nd	7·92	6·17	5·13	6·34	7·98	5·83	4·06	3·44	4·06	5·01	6·85	5·77
Sm	2·38	1·97	1·59	2·00	2·50	1·79	1·36	1·19	1·36	1·47	2·33	2·00
Eu	0·820	0·778	0·654	0·676	0·801	0·794	0·483	0·441	0·487	0·406	0·823	0·701
Gd	3·05	2·43	2·07	2·50	3·01	2·35	1·81	1·51	1·79	2·05	2·88	2·50
Tb	0·483	0·422	0·325	0·401	0·516	0·373	0·301	0·278	0·301	0·312	0·503	0·441
Dy	3·28	2·85	2·22	2·67	3·40	2·61	2·08	1·89	2·06	2·19	3·27	2·95
Ho	0·700	0·646	0·485	0·583	0·755	0·583	0·455	0·427	0·457	0·489	0·720	0·659
Er	2·11	1·92	1·50	1·79	2·21	1·78	1·38	1·24	1·37	1·52	2·04	1·89
Tm	0·319	0·292	0·219	0·250	0·326	0·271	0·197	0·190	0·201	0·226	0·287	0·270
Yb	2·27	2·12	1·56	1·85	2·34	1·99	1·42	1·30	1·44	1·66	2·05	1·90
Lu	0·359	0·343	0·244	0·287	0·369	0·316	0·220	0·203	0·213	0·265	0·325	0·302
Hf	1·38	1·30	1·00	1·07	1·29	1·29	0·76	0·64	0·74	1·25	1·20	1·10
Ta	0·052	0·058	0·042	0·044	0·059	0·054	0·022	0·054	0·031	0·036	0·038	0·035
Pb	3·85	3·72	2·21	3·85	4·98	2·78	2·11	1·76	2·32	4·55	2·34	3·20
Th	0·437	0·427	0·305	0·340	0·458	0·379	0·169	0·147	0·157	0·305	0·245	0·212
U	0·409	0·355	0·276	0·365	0·361	0·359	0·161	0·125	0·158	0·265	0·170	0·134
Ti	3540	3300	3900	3960	3600	3360	3600	3060	3300	2340	4980	4680
F	—	—	—	69	—	—	90	—	—	86	80	68
CO_2	—	—	—	280	—	—	330	—	—	330	320	270
H_2O^+	—	—	—	0·68	—	—	0·56	—	—	0·43	0·42	0·41

Island:	TONGA Kao				Tofua	Hunga Ha'apai		Hunga Tonga		
Sample:	T103C	104C	64 T4C	64 T6	Tof32	HHBF (HH1)	HHUF	38982	38983	38984
Rock type:	BA	BA	BA	BA	D	BA	BA	A	BA	BA
Li	4·27	3·97	6·1	4·3	5·43	4·39	5·42	6·05	5·19	3·77
Be	0·30	0·36	0·31	0·30	0·29	0·20	0·22	0·27	0·20	0·19
Sc	35·4	40·0	35·3	33·8	41·2	38·5	47·1	43·5	52·4	52·2
V	293	313	330	315	368	290	335	367	343	348
Cr	26·4	36·0	25·7	26·2	11·3	44·5	52·0	8·30	52·5	53·4
Co	42·4	45·2	33·6	33·4	40·5	35·1	40·6	—	—	—
Ni	24·4	32·4	25·2	25·9	18·7	28·2	37·3	16·7	36·1	41·6
Cu	136	108	113	105	143	137	157	204	162	190
Zn	80·1	96·4	82·0	85	107	75·2	79·6	—	83·8	90·7
Ga	16·8	17·2	15·6	16·1	17·4	16·7	15·9	15·4	15·4	15·6
Rb	6·66	6·57	5·83	5·79	8·46	4·20	5·88	6·52	5·95	5·50
Sr	244	266	234	231	242	189	179	171	178	181
Y	17·5	18·2	20·9	20·8	20·0	12·5	12·6	16·7	14·2	14·4
Zr	38·9	41·3	46·0	45·3	36·2	20·2	22·5	37·0	22·7	22·7
Nb	0·38	0·42	0·43	0·40	0·36	0·25	0·28	0·67	0·49	0·40
Cs	0·22	0·19	0·23	0·23	0·38	0·22	0·29	0·43	0·36	0·28
Ba	123	113	119	120	186	110	126	197	129	118
La	2·27	2·45	2·29	2·36	2·31	1·32	1·09	1·67	1·69	1·77
Ce	6·80	7·25	6·51	6·62	6·76	3·87	3·50	6·02	4·65	4·88
Pr	1·19	1·29	1·13	1·17	1·15	0·610	0·541	0·893	0·813	0·853
Nd	6·01	6·55	6·06	6·16	6·02	3·33	3·08	4·53	4·04	4·21
Sm	2·00	2·11	2·09	2·12	2·05	1·18	1·13	1·61	1·37	1·42
Eu	0·728	0·795	0·741	0·753	0·744	0·430	0·472	0·582	0·534	0·538
Gd	2·62	2·75	2·61	2·67	2·83	1·65	1·60	2·41	1·97	2·01
Tb	0·430	0·447	0·472	0·486	0·469	0·287	0·281	0·412	0·333	0·340
Dy	2·92	3·05	3·08	3·16	3·19	2·00	2·00	2·94	2·34	2·37
Ho	0·633	0·664	0·698	0·700	0·699	0·448	0·451	0·657	0·528	0·526
Er	1·91	1·97	1·99	2·00	2·13	1·38	1·40	2·04	1·61	1·60
Tm	0·269	0·285	0·282	0·283	0·309	0·197	0·207	0·295	0·228	0·232
Yb	1·89	1·97	2·02	2·03	2·17	1·41	1·52	2·08	1·62	1·62
Lu	0·291	0·298	0·313	0·318	0·338	0·220	0·241	0·326	0·256	0·256
Hf	1·19	1·27	1·19	1·21	1·22	0·67	0·76	1·24	0·761	0·749
Ta	0·034	0·038	0·038	0·031	0·025	0·018	0·022	—	—	—
Pb	1·67	2·47	1·93	2·25	2·69	1·39	1·80	—	—	—
Th	0·203	0·211	0·213	0·214	0·224	0·121	0·143	0·224	0·162	—
U	0·156	0·181	0·145	0·139	0·217	0·130	0·142	0·307	0·180	—
Ti	4740	4980	5040	4980	4620	2940	3660	4500	3480	3480
F	88	88	75	72	85	81	—	—	—	—
CO_2	340	330	280	280	320	310	—	—	—	—
H_2O^+	0·34	0·38	0·47	0·40	0·31	0·33	—	—	—	—

Table A1: continued

Island:	TONGA Niua fo'ou			KERMADECS Raoul Group						
Sample:	N107	N111	N131	7005	7101	14775	14782	14790	14796	23374
Rock type:	B	B	B	D	B	BA	B	BA	BA	BA
Li	6·0	—	—	—	4·74	3·64	4·70	6·15	5·35	—
Be	0·67	0·49	0·50	0·39	0·28	0·20	0·29	0·27	0·23	0·18
Sc	46·0	45·6	48·2	21·2	34·8	36·9	48·4	36·7	38·3	47·6
V	300	288	301	43·5	329	329	316	294	299	307
Cr	207	319	345	0·38	24·3	47·5	106	17·8	8·85	152
Co	41·4	42·3	43·9	31·3	42·3	40·6	51·6	38·6	38·2	48·5
Ni	44·6	57·5	61·2	1·35	20·5	23·7	40·3	19·2	16·1	35·7
Cu	73·0	84	77	—	97·8	188	153	175	145	117
Zn	83·0	82	81	—	84·8	79·4	88·6	87·6	81·0	85·0
Ga	18·0	16·8	16·8	13·9	19·0	16·8	16·0	17·6	18·3	14·0
Rb	3·43	2·67	3·02	9·03	4·83	1·35	1·11	5·21	4·76	3·91
Sr	172	165	160	151	205	151	160	159	166	143
Y	41·1	32·9	33·5	37·7	15·6	16·5	15·3	19·4	16·8	17·4
Zr	128	95·8	96·9	68·1	27·5	28·6	28·8	39·7	31·0	30·6
Nb	4·68	3·53	3·75	0·68	0·37	0·35	0·31	0·37	0·29	0·28
Cs	0·037	0·035	0·038	0·76	0·35	0·037	0·032	0·37	0·32	0·25
Ba	45·6	32·8	35·3	199	86·0	52·0	31·5	101	88·5	74·7
La	5·56	4·21	4·27	3·90	2·26	1·12	1·37	1·84	1·50	1·54
Ce	15·86	12·1	12·2	10·9	6·45	3·92	4·59	5·92	5·04	4·49
Pr	2·58	1·98	2·01	1·82	1·07	0·660	0·792	1·02	0·870	0·774
Nd	13·2	10·2	10·1	9·82	5·53	3·70	4·37	5·38	4·57	4·23
Sm	4·31	3·41	3·43	3·46	1·81	1·44	1·63	1·94	1·67	1·54
Eu	1·50	1·23	1·24	1·05	0·689	0·529	0·619	0·689	0·647	0·541
Gd	5·40	4·32	4·31	4·46	2·36	1·90	2·19	2·66	2·36	2·09
Tb	0·981	0·785	0·795	0·826	0·403	0·338	0·380	0·472	0·412	0·382
Dy	6·38	5·11	5·13	5·49	2·68	2·32	2·60	3·26	2·88	2·60
Ho	1·39	1·12	1·13	1·25	0·577	0·507	0·564	0·71	0·63	0·581
Er	3·91	3·12	3·15	3·63	1·75	1·55	1·64	2·18	1·89	1·66
Tm	0·537	0·428	0·429	0·524	0·242	0·215	0·232	0·309	0·275	0·233
Yb	3·76	3·05	3·09	3·78	1·67	1·510	1·63	2·20	1·94	1·70
Lu	0·584	0·466	0·470	0·594	0·263	0·229	0·238	0·337	0·294	0·265
Hf	2·73	2·09	2·13	1·99	0·95	0·76	0·974	1·34	1·10	0·866
Ta	0·27	0·20	0·22	—	0·024	0·022	0·025	0·031	0·025	—
Pb	1·16	0·70	1·07	3·25	1·69	1·40	1·75	2·06	1·76	1·52
Th	0·444	0·329	0·338	0·578	0·245	0·161	0·167	0·282	0·255	0·249
U	0·106	0·094	0·090	0·220	0·120	0·088	0·076	0·146	0·120	0·090
Ti	10670	8210	8450	3660	5040	4620	4740	4860	4440	3780
F	—	82	76	—	74	—	—	—	—	68
CO_2	—	310	—	—	—	—	—	—	—	—
H_2O^+	—	0·44	0·44	—	—	—	—	—	—	0·94

Island:	KERMADECS Raoul Group			Macauley					Curtis	
Sample:	23376	23383	23386	10378	10379	10380	10384	10415	14849	14864
Rock type:	BA	BA	A	B	B	B	D	B	D	D
Li	5·2	—	—	—	3·84	—	10·7	3·15	—	3·12
Be	0·26	0·18	0·22	0·42	0·28	0·36	0·83	0·15	0·45	0·50
Sc	42·8	39·1	31·7	41·1	35·2	48·8	12·9	46·1	23·7	21·6
V	286	298	273	345	269	411	9·9	280	61·5	92·7
Cr	184	27·3	12·6	24·7	54·3	72·3	1·01	159	0·65	1·13
Co	44·0	42·1	31·6	40·3	45·3	47·0	6·9	50·4	6·75	11·6
Ni	42·1	17·9	12·6	26·8	41·4	38·6	3·33	56·2	1·36	2·83
Cu	108	90·0	51·0	125	139	185	31·8	107	10·0	24·0
Zn	92·0	101	93·0	75·0	64·3	87·0	83·4	59·4	150	76·1
Ga	14·2	15·7	16·6	15·9	17·7	16·3	15·5	15·7	15·5	15·0
Rb	4·56	2·87	3·10	10·5	7·35	8·16	27·4	2·83	5·86	12·0
Sr	166	131	169	277	276	236	162	203	201	171
Y	17·9	20·2	23·6	14·8	11·6	17·2	38·0	9·62	24·4	35·0
Zr	38·2	30·7	29·2	36·0	25·7	38·4	126	16·6	68·6	71·2
Nb	0·50	0·34	0·30	0·56	0·44	0·57	1·63	0·22	0·66	0·65
Cs	0·26	0·26	0·11	0·36	0·26	0·32	1·30	0·13	0·58	0·98
Ba	94·7	129	89·5	123	104	126	399	49·1	245	274
La	2·61	1·69	1·63	3·80	2·96	4·68	10·1	1·05	2·89	4·34
Ce	7·12	4·65	4·95	9·42	7·70	9·94	27·8	3·48	8·10	12·1
Pr	1·16	0·813	0·879	1·44	1·21	1·55	4·09	0·536	1·36	2·03
Nd	5·84	4·04	5·41	7·10	5·69	7·72	19·7	3·09	7·12	10·9
Sm	1·93	1·37	2·00	2·13	1·70	2·33	5·07	1·12	2·56	3·71
Eu	0·646	0·534	0·740	0·736	0·620	0·793	1·36	0·417	1·06	1·09
Gd	2·38	1·97	2·78	2·36	1·99	2·66	5·99	1·401	3·10	4·44
Tb	0·412	0·333	0·525	0·377	0·315	0·431	0·97	0·240	0·580	0·802
Dy	2·70	2·34	3·54	2·38	1·99	2·73	6·53	1·58	3·94	5·34
Ho	0·602	0·528	0·793	0·494	0·416	0·58	1·40	0·330	0·863	1·17
Er	1·73	1·61	2·31	1·38	1·24	1·65	4·37	1·00	2·55	3·45
Tm	0·243	0·228	0·332	0·188	0·166	0·220	0·623	0·137	0·367	0·540
Yb	1·76	1·62	2·40	1·35	1·17	1·62	4·46	0·971	2·78	3·56
Lu	0·272	0·256	0·373	0·210	0·178	0·247	0·677	0·147	0·434	0·541
Hf	1·05	0·761	0·932	0·888	0·78	1·02	4·16	0·53	2·03	2·13
Ta	0·040	—	—	0·035	0·024	0·035	0·108	0·017	0·042	0·066
Pb	1·56	1·18	1·73	1·60	1·68	2·25	7·15	0·907	16·9	5·14
Th	0·382	0·166	0·191	0·501	0·395	0·581	1·71	0·131	0·712	0·738
U	0·138	0·096	0·076	0·225	0·177	0·180	0·695	0·082	0·271	0·563
Ti	3840	4080	4260	4200	3720	5340	3900	3300	4500	3420
F	79	72	70	—	—	—	—	79	—	—
CO_2	310	260	260	—	—	—	—	300	—	—
H_2O^+	0·36	1·08	0·25	—	—	—	—	0·37	—	—

Table A1: continued

Island:	KERMADECS Curtis	L'Esperance			
Sample:	14868	14831	14835	14837	14840
Rock type:	R	BA	BA	BA	BA
Li	4·41	—	5·3	0·83	3·41
Be	0·51	0·35	0·37	0·32	0·37
Sc	17·4	36·2	39·0	38·7	37·2
V	24·6	350	436	356	331
Cr	0·29	4·96	6·33	11·7	5·29
Co	7·0	34·7	39·1	43·5	41·5
Ni	1·67	10·5	12·2	18·6	12·8
Cu	13·7	8·0	69·2	79·4	30·3
Zn	71·2	107	98·8	107	127
Ga	14·3	18·0	18·5	19·6	19·9
Rb	6·99	6·99	10·7	8·84	7·45
Sr	173	220	229	220	243
Y	38·0	22·4	22·5	16·9	20·2
Zr	84·5	40·9	41·8	28·8	39·7
Nb	8·74	0·45	0·50	0·40	0·46
Cs	0·79	0·42	0·35	0·47	0·35
Ba	338	136	152	127	151
La	4·92	3·30	3·36	2·73	3·32
Ce	13·3	8·76	9·01	7·63	9·12
Pr	2·14	1·41	1·45	1·26	1·50
Nd	11·3	7·32	7·51	6·21	7·33
Sm	3·84	2·39	2·45	1·92	2·32
Eu	1·14	0·891	0·894	0·803	0·909
Gd	4·67	3·00	2·95	2·45	3·02
Tb	0·822	0·520	0·503	0·410	0·490
Dy	5·50	3·44	3·32	2·79	3·33
Ho	1·21	0·770	0·722	0·590	0·717
Er	3·58	2·20	2·08	1·78	2·11
Tm	0·567	0·305	0·317	0·248	0·309
Yb	3·75	2·19	2·08	1·73	2·10
Lu	0·571	0·341	0·315	0·260	0·325
Hf	2·45	1·13	1·15	0·90	1·24
Ta	—	0·035	0·048	0·035	0·033
Pb	7·03	2·92	2·85	2·22	2·39
Th	0·911	0·608	0·581	0·504	0·543
U	0·869	0·441	0·202	0·181	0·213
Ti	3300	6300	6300	6060	6000
F	—	—	—	85	—
CO_2	—	—	—	330	—
H_2O^+	—	—	—	0·54	—

Major element analyses of samples have been presented by Ewart *et al*. (1973, 1977, 1994*a*) and J. A. Gamble (personal communication, 1994) for the additional Tafahi and Niuatoputapu samples. B, basalt; BA, basaltic andesite; A, andesite; D, dacite; R, rhyolite.